THESIS

BISTABLE PRESTRESSED SPRING STEEL GRIPPERS FOR AERIAL PERCHING AND GRASPING

Submitted by

Bryce Jones

Department of Mechanical Engineering

In partial fulfillment of the requirements

For the Degree of Master of Science

Colorado State University

Fort Collins, Colorado

Fall 2024

Master's Committee:

Advisor: Jianguo Zhao

Marco Ciarcia
Steve Simske

ABSTRACT

BISTABLE PRESTRESSED SPRING STEEL GRIPPERS FOR AERIAL PERCHING AND GRASPING

Quadcopter drones are popular in both the consumer and commercial markets, with a wide range of uses and applications, including inspections, research, natural disaster response, and filming and photography. These uses and applications are currently limited, however, by the limited battery power and range of current drones. Aerial perching can extend the useful flight time of a drone by allowing for passive perching in a location for a desired amount of time. Compliant bistable mechanisms are well-suited for this application because of their adaptability in a wide range of environments while utilizing bistability to reduce energy consumption and complexity. Current research into aerial perching with compliant mechanisms is limited to heavy, rigid grippers with limited applications in a wide variety of environments and grippers with complicated pneumatic controls.

In this thesis, we propose a novel solution to this gap in research through the use of prestressed spring steel bands (PSSB) to create compliant bistable grippers for aerial perching and grasping. We investigate multiple different PSSB configurations. We first investigate two single PSSB gripper designs, a single band gripper with a cable driven opening system, then an improved silicone encased single PSSB gripper design. The first single band gripper is experimentally tested to determine the triggering force, effect of offset on triggering force, effect of spring pretension on triggering force, opening force, grasping force, and activation time. This design had some issues with opening reliably and tangling. The improved silicone encased gripper is experimentally tested for triggering force, the effect of varying contact points and angles, activation time, reduction of triggering force with springs, and actual flight tests on a drone done in partnership with IIIT Hyderabad. The single band gripper designs can grasp a variety of objects, especially cylindrical ones,

but are limited in grasping spherical and heavier objects, and vertical grasping. We then design a cross-shaped gripper based on the silicone encased PSSB gripper. This gripper is experimentally tested in the same manner as the silicone encased single band gripper and performs well in grasping spherical objects and vertical grasping. It does, however, struggle to grasp longer cylindrical objects. These gripper designs have a fixed triggering force based on the design that limited the applications for drone applications with high acceleration causing inadvertent activation, as well as for grasping lightweight objects. Being able to actively control the triggering force of the grippers would give the ability to tune the gripper for ideal performance in a wide range of applications. To actively tune the triggering force, we investigate the use of on the fly tuning with Nitinol Shape Memory Alloy springs. We first attempted closed-loop control by using a PID controller to control the resistance of the springs. Then we used an open loop control method where constant voltage is applied to the springs that allows for precise tuning of the triggering force to a set range for the desired application, and experimentally verify the reduction in triggering force and show the application of on the fly triggering force tuning.

ACKNOWLEDGEMENTS

First, I would like to thank my friends, family, and girlfriend for all of their continued support throughout this entire process. I would not be in the position that I am today without all of your help, guidance, and encouragment.

I would also like to thank my peers in the lab who helped me many times over the years to solve complex and challenging problems, especially Clint Middlemist, Sydney Speigel, Mahmud Saikot, and Eli Lerner. I would like to thank all of the professors who dedicated their time to teaching me both undergrad and graduate courses, you are the reason I am the engineer that I am today. I also want to thank Dr. Steven Simske and Dr. Marco Ciarcia for their time, guidance, and honest feedback as committee members for my work.

Finally, I would like to extend my heartfelt gratitude to Dr. Jianguo Zhao for giving me the opportunity to work in the Adaptive Robotics Laboratory. His mentorship has been instrumental in my growth as a researcher and engineer. Over the past two and a half years, he has helped me build confidence in my strengths and improve my weaknesses. Dr. Zhao consistently challenged me to exceed my expectations, and with his guidance, I repeatedly rose to the occasion.

I believe that I would not be the person and engineer that I am now without the support and guidance from everyone mentioned. Thank you for all of your help.

DEDICATION

I want to dedicate this thesis to my parents, Brian and Devon, for their never-ending support and commitment to my success, and for always pushing me to be the best version of myself. I know how many late nights and weekends you both spent working, and how hard you have worked to provide for me and my brother over the years. I will never be able to express how thankful I am to you both.

TABLE OF CONTENTS

LIST OF FIGURES

Chapter 1

Introduction

1.1 Background and Previous Work

The goal of this research is to develop novel compliant bistable prestressed spring steel band (PSSB) grippers for aerial perching and grasping with drones that do not require precise motion control and experimentally characterize and validate their performance. Additionally, we investigate and utilize Nitinol Shape Memory Alloy (SMA) springs to tune the triggering force of these grippers on the fly. The following sections describe the required background and previous research to understand aerial manipulation and grasping, compliant and bistable mechanisms, prestressed spring steel, and the applications of Nitinol Shape Memory Alloys.

1.1.1 Aerial Manipulation and Grasping

Aerial grasping, the field that enables flying robots to pick up, manipulate, and execute specific tasks with various objects, has gained traction in recent years. This heightened interest is primarily attributed to the advantages it offers compared to the conventional ground-based counterparts. Their high accessibility and mobility make them suitable for diverse applications such as transportation, inspection and maintenance of structures, rapid deployment of emergency supplies in disaster response, precision agriculture, etc [9–12]. These applications are currently limited, however, by the limited battery power and range of current drones. Due to the low energy densities of current Lithium-Ion batteries, it is common for drones to have 15-25 minutes of useful flight time on a single battery before they have to recharge [13]. Aerial perching can extend the useful flight time of a drone by allowing for passive perching in a location for a desired amount of time. This will conserve the battery when compared to flight and hovering uses, allowing for power to be used for other applications during perching. To achieve perching in a wide variety of environments, a compliant bistable mechanism is needed that can passively perch a drone.

Successful aerial grasping emerges from good motion control together with proper gripper design. The gripper's design plays a major role in determining the success of the aerial grasping systems. If properly designed, the gripper can alleviate the requirement for precise motion control [8, 14, 15]. Another metric for successful grasping is the ability to secure the grasp rapidly and without dislodging or moving the object being grasped. To achieve this, many grippers utilize a triggering mechanism that will trigger the gripper upon contact [3, 4, 16–19]. Some of these mechanism have high triggering or contact forces, leading to issues with moving or dislodging the object. Reducing this triggering force or making the triggering mechanism adaptive and tunable is one method of making grasping more successful

1.1.2 Bistable and Compliant Mechanisms

As the goal of this research is to develop a compliant bistable gripper, it is important to understand what a compliant bistable mechanism is. A bistable mechanism is a mechanism that has two stable equilibrium positions, where it will remain in either position without any external forces [20]. Common examples include light switches and binder rings. The advantage of bistable mechanisms is the ability to have 2 equilibrium positions with no external forces or power required. Aerial perching and gripping can utilize bistable mechanisms to achieve passive perching with no activation control systems or power use during perching.

A compliant mechanism is a mechanism that gains much "of its mobility from the deflection of flexible members rather than from movable joints" [20]. These mechanisms use designed flexibility to achieve complex motion instead of movable joints. The largest advantage of compliant mechanisms is simplicity, reliability, and a reduction in part quantities and mass. Outside of robotics, compliant mechanisms are common in micro-electro-mechanical system (MEMS) applications, such as accelerometers in smartphones [21]. A compliant mechanism is well suited for use in aerial grippers because it allows for a single gripper to adapt to different perching conditions. While compliant mechanisms have many advantages for use in aerial grippers, there are still disadvantages. These include fatigue resistance, which limits the lifetime of compliant mechanisms.

The material properties and design of the mechanism also limit its strength, as the mechanism must be designed to be flexible [20]. When compliancy is combined with a bistable mechanism, a compliant bistable mechanism that has 2 equilibrium positions that are actuated with designed flexibility is created.

1.1.3 Material and Mechanical Properties of Prestressed Spring Steel

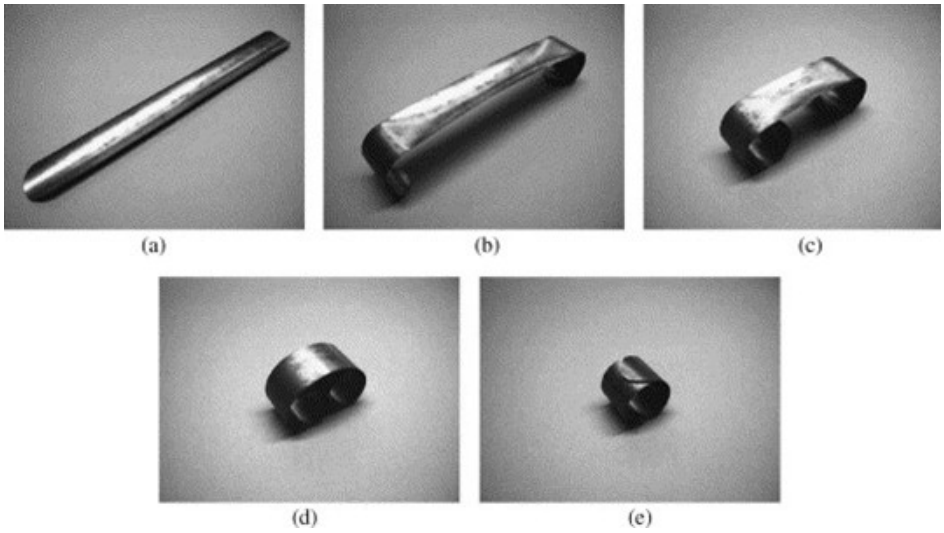

Figure 1.1: Bistable configurations of a PSS band (a and e) and transition between bistable configurations [1]

The material and mechanical properties of the gripper are integral to the functionality and performance of the gripper. The gripper must be made from a material that is both compliant and flexible while maintaining the ability to hold the weight of the drone. The material that will be used in this research is prestressed spring steel bands (PSSB), because of its elastic, strength, and bistable properties. PSS is steel that is manufactured to have a "particular distribution of residual stress induced by plastic bending" [1]. When manufactured into a long band, in the form of a semi-cylindrical surface, unique properties are observed. The band has 2 stable configurations, a flattened, and rolled-up position, which can be seen in Fig. 1.1 in images (a) and (e). When a large enough external force is applied to the band in the flattened position, it will rapidly transition to the rolled-up state, as seen in Fig. 1.1, images (b-d). To transition from the rolled-up state back

to the flattened state, an external force will be applied to the ends of the band. Currently, a thin cable is being tested as a method to unroll the band. Modeling of these bands can be done using the method presented in [1] and [22] to estimate the mechanical and material properties. Common examples of this type of PSS band include tape measures and slap bracelet toys.

1.1.4 Nitinol Shape Memory Alloys

To control and tune the triggering force of the PSSB grippers, we will utilize the unique properties of Nitinol Shape Memory Alloy (SMA) springs. Nitinol SMA's have unique properties that make it very useful for a wide range of applications. These range from medical devices [2, 23–25], deep sea ocean engineering [26–28], aerospace components [29–31], and robotic actuation [6,27,32,33]. Nitinol, or Equiatomic Nickel-Titanium (NiTi) alloys, have unique shape memory features due to changes in the crystalline structure of the alloy when heat is applied [34, 35]. When cold, Nitinol alloys are in the martensite forms and are easily yielded and deformed into a desired shape [34, 35]. Nitinol SMA's have the ability to recover strains up to 8 percent and return their original shape when heated past the transformation temperature [2, 35]. When Nitinol is heated past the transformation temperature, the crystalline structure changes from martensite to austenite and returns to its original 'trained' shape with substantial force generation [23,34]. When the Nitinol cools after heating it will again pass the transformation temperature and transition from austenite back to a martensite crystal structure. This phase change is detailed in Fig. 1.2. Nitinol SMA springs will be used to control and tune the triggering force of the grippers. This will be done using the unique force generating phase transitions as the springs are heated.

1.1.5 Previous Aerial Grasping Research

Many grippers have been recently designed for aerial grasping, and some important recent research is outlined here. Several research groups have developed passive grippers, often featuring two or three fingers. Notable examples include grippers leveraging pre-stored potential energy [36] and von Mises bistable mechanisms [3, 14]. Zhao, *et al*. [3] developed a mechanically intelligent and passive (MIP) gripper that can passively perch and grasp small-diameter objects. This grip-

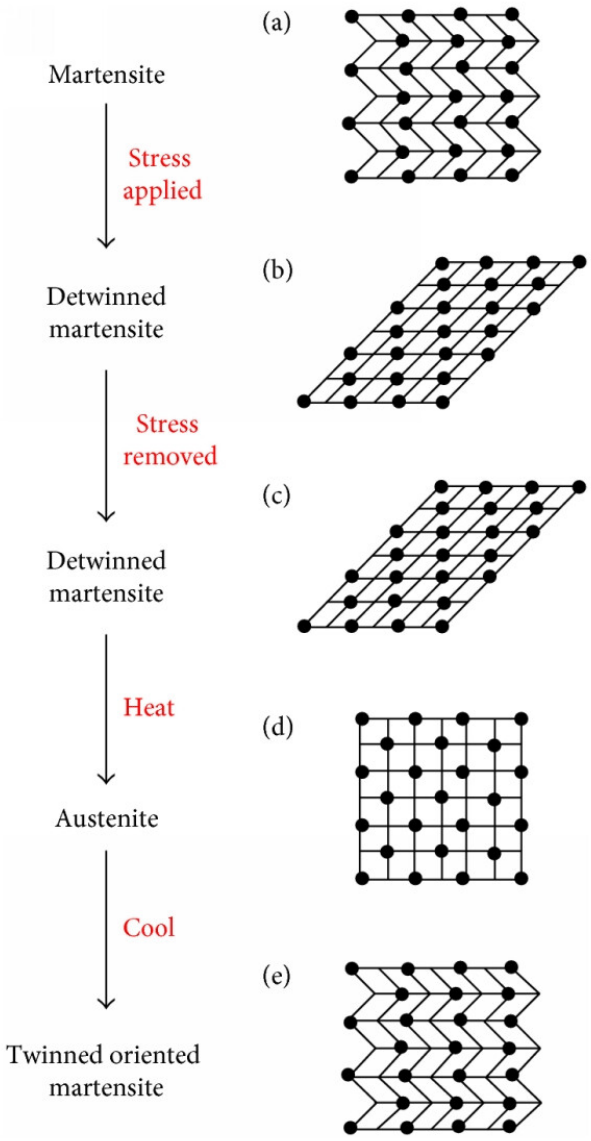

Figure 1.2: Phase change for Nitinol SMA where a) original martensite crystal structure, b-c) deformed martensite crystal structure during and after stress is applied and removed, d) austenite crystal structure during heating past transformation temperature causing shape memory affect, and e) final cooled martensite structure after shape recovery [2]

per uses mechanical intelligence, allowing it to "not need precise control for both perching and releasing" [3]. The gripper can hold 132 times its mass, as seen in Fig. 1.3, which shows the mechanically intelligent design working to hold a 2.77 kg kettlebell and 3.7 kg bucket of water. The gripper, however, is limited to grasping a small, fixed maximum diameter, as the structure of the

gripper is rigid and non-compliant. This limits the realistic functionality of the MIP gripper. These grippers, while adept at perching, have limitations when grasping objects of different shapes.

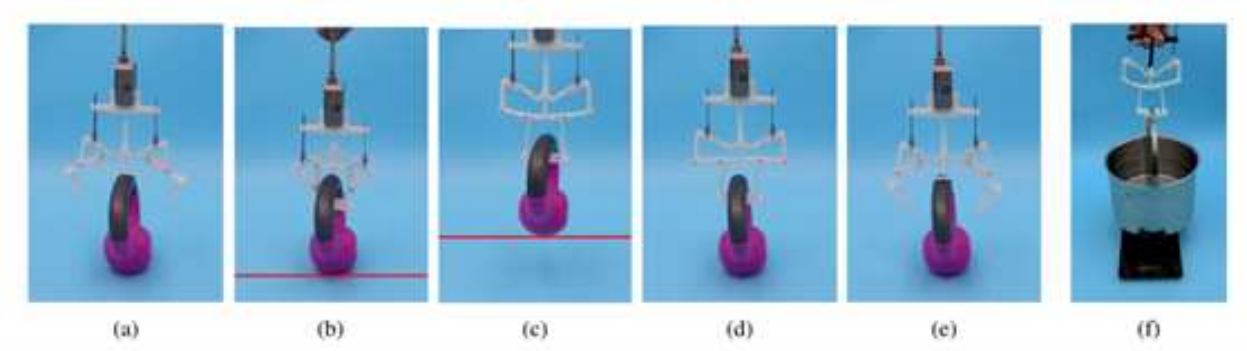

Figure 1.3: MIP Gripper Grasping and Release Process with a Kettlebell and Water Bucket [3]

Other designs for passive grippers, such as the high-speed gripper [37], bistable claw gripper [17], bird-inspired robotic leg and claw gripper [38], utilize claw-like mechanisms to enable grasping. There has also been research into emulating grippers that are seen in nature. Geckeler, *et al*. [4] designed a helical origami gripper that uses folding origami to achieve passive perching through its bistable configurations. The gripper is based on animal tails, like spider monkeys, opossums, and snakes that can coil around tree branches for perching or grasping. The gripper can hold up to 2.8 N, which is more than 50 times its weight [4]. The gripper, however, was designed for use in sensor placement and is currently not electrically resettable for use in a drone.

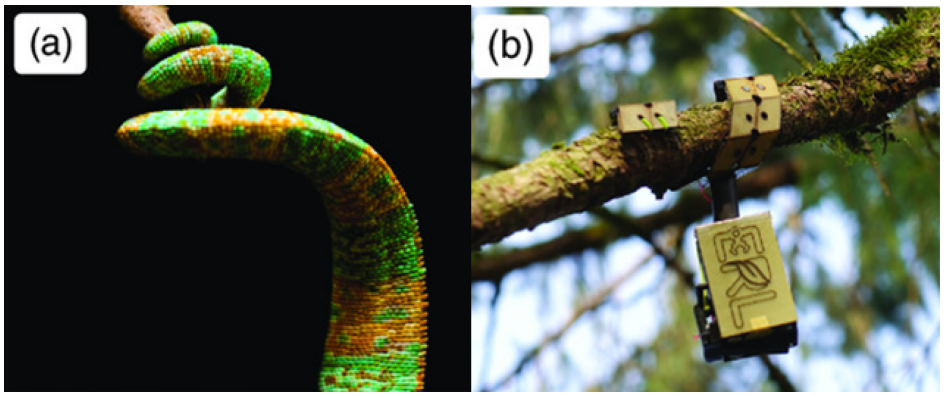

Figure 1.4: Helical Origami Gripper (b) compared to a coiled animal tail [4]

Another bio-inspired gripper can be seen in the micro spine grapple developed by Nguyen, *et al*. [39]. The grapple is attached by flying the drone over the perching surface from the side so that the hanging microspine grapple can make sufficient contact, with the drone then hanging below the perch. The grapple is compliant to accept many different perching geometries and can support up to 60 kilograms in ideal conditions. It is limited by heavy, complicated control systems and requires a 2-meter radius around the grapple for successful perching, limiting functionality [39].

However, these bio-inspired gripper designs can be quite complex and may encounter reliability issues. In contrast to passive grippers, some grippers adopt an active approach, such as servo motors or artificial tendons for controlling the gripper. Examples of these grippers include the hybrid manipulator/gripper [40], the soft fin-ray structure-based gripper [41], and the tendon actuated soft gripper [42]. The active energy consumption of these grippers poses a challenge since efficient energy utilization is critical in aerial applications. To address these issues, researchers have sought to simplify the gripper designs using pre-stressed bistable beams (PSSB) [5, 18, 43]. Wang, *et al*. [43] developed a PSSB bistable pneumatic gripper that is inspired by Venus Flytrap motion. The gripper consists of 2 pressure chambers that are on top and bottom of a PSSB. To actuate the gripper, the top pressure chamber is inflated to 50 kPa, transitioning the PSSB from the flattened to rolled configuration [43]. To return the PSSB to the flattened configuration, the bottom pressure chamber is inflated to 140 kPa [43]. The pressure input can then be removed, allowing the PSSB to hold a maximum mass of 344 grams [43]. While the gripper is compliant and bistable, it has thus far only been tested with grasping objects and is limited by complex and heavy pneumatic control systems.

Furthermore, Nguyen, *et al*. [5] developed a pneumatic compliant bistable PSSB gripper for perching of drones. The PSSB is activated by the downward motion of the drone and is returned to its flattened state by inflating the pneumatic chamber, which takes about 3 seconds and 83 kPa [5]. Holding up to 176 N in ideal conditions, the gripper works well for perching drones, as seen in Fig. 1.5 [5]. Its complex pneumatic control systems, however, are heavy and limit the functionality and battery of smaller drones. Additionally, Jitosho, *et al*. [18] developed a similar

pneumatic compliant bistable PSSB gripper to [5]. It is actuated by contact force and is returned to the flattened state by inflating the pneumatic chamber, which takes about 15 seconds [18]. The gripper has thus far only been tested for grasping objects and not for perching. Complex and heavy pneumatic control systems and long inflation times limit the functionality for use in drone perching.

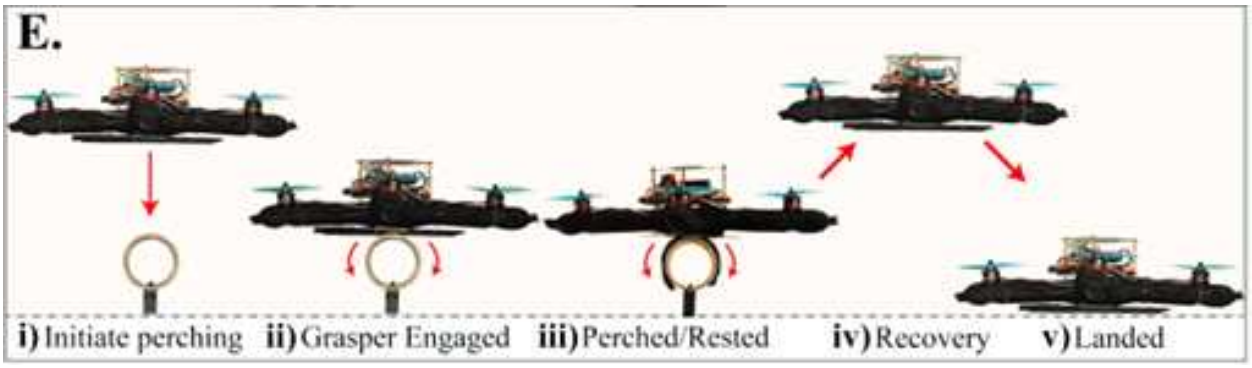

Figure 1.5: Perching and recovery process for compliant bistable PSSB gripper [5]

1.1.6 Previous Nitinol Force Generation research

Nitinol SMA has recently been used in numerous robotic grippers and actuators due to their ability to generate force and motion. The most common use of Nitinol SMA's for these applications is for actuation, either through Nitinol wire or springs. Springs are used to generate force and motion for actuation in [6, 44–46], where the springs are heated to compress to the 'memorized' coiled spring shape. The SMA spring motion pulls on a part of the grippers to create the desired actuation. This can be clearly seen in Fig. 1.6, where the SMA springs actuate from a stretched state to a coiled state when heated to actuate a finger on a TPU hand [6]. The SMA springs have very high displacement and elongation due to the coiled nature of the springs [6]. The coiled springs also create one of the downsides of SMA springs, which is reduced force generation compared to SMA wire [7, 47]. Nitinol SMA wire is used for robotic actuation in [7, 32, 48, 49]. These actuators have limited displacement of 3 to 8 percent of their length but have very high force generation compared to SMA springs [7, 47]. In Fig. 1.7, SMA wire is utilized to actuate and

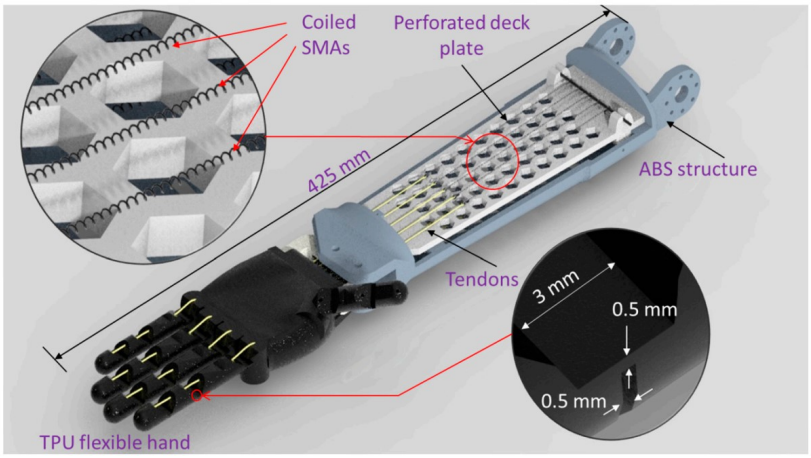

Figure 1.6: TPU hand actuated by 10 SMA springs, with a flexor and extensor SMA spring actuator for each finger [6]

close a gripper through the contraction of the SMA wire as it is heated [7]. This design routes the SMA wire around 9 pegs to increase the length, which allows for more total displacement. The SMA wires contract about 4 percent of its original 67 mm length and produce up to 19.61 N of force. [7]. There have also been many research efforts in [47, 50, 51] into numerical modeling and

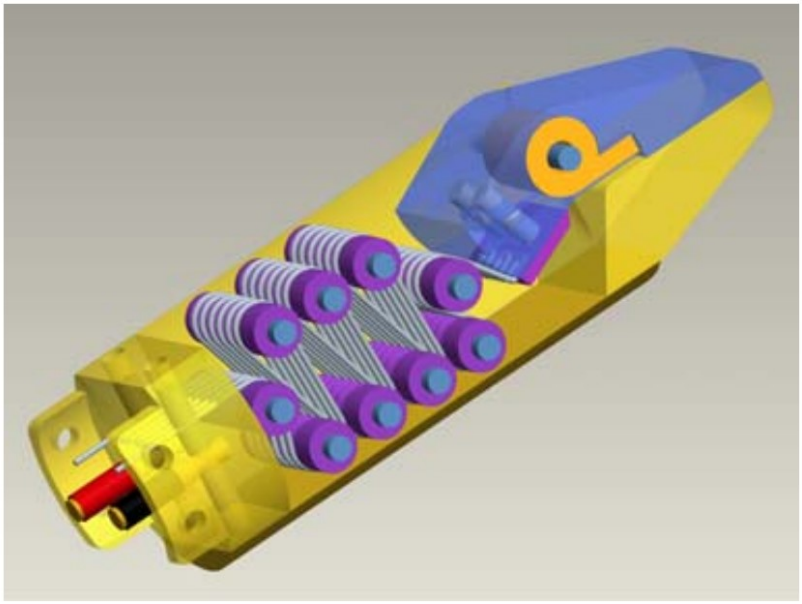

Figure 1.7: SMA Wire gripper design that utilizes contraction of SMA wire to actuate a gripper [7]

analysis of Nitinol SMA material. Controlling the displacement and deflection of SMA spring

actuators through Finite Element Analysis (FEA), numerical, and experimental validation is done in [51]. Similarly, [50] focuses on controlling the strain elongation percentage of SMA springs for varying applied stresses and forces through the Souza-Auricchio, modified Souza-Auricchio, and Auricchio-Bonettie models. Hybrid models that aim to characterize the relationship between current, force, elongation, and temperature are created in [47]. This work is valuable because it combines all real-world parameters that affect Nitinol SMA dynamics and performance into one hybrid model [47].

1.1.7 Gap in Current Research

This research aims to develop a functional lightweight compliant bistable PSSB gripper for passive perching in a wide variety of environments. It is important to discuss the gap in the current research that the proposed novel grippers will address. The grippers in [3], [4], [17], [38], [37] and [39] demonstrated the functionality of passive grippers for perching applications but have limited applications in a variety of environments. Compliant bistable PSS grippers in [18], [43], and [5] show that PSS can functionally be used for passive grasping and perching on a wide variety of shapes and geometries. Current research on compliant bistable PSS grippers, however, uses relatively heavy and complicated pneumatics to actuate the PSS and return it to a flat configuration. This limits functionality and excludes potential use in small drones because of the increased weight. To reduce weight, a simpler control system using a small motor and thin cables will be used to actuate the PSS and return it to the flat configuration.

To the best of the author's knowledge, Nitinol SMA springs have never been used to reduce the triggering force of a gripper in this manner, only for actuation purposes in robotic actuation as shown in [7, 44–46, 48, 49].

1.2 Contributions

- **Novel Single Prestressed Spring Steel Band Gripper Designs:** We present two single PSSB gripper designs that allow for versatile grasping in a variety of environments. The

first gripper utilizes a single PSSB with a cable opening system and grip tape to create high grasping force and grasping success for varying parameters. We then improve on this gripper design by creating a more compact and lightweight gripper design with a silicone encased PSSB. This design implements a unique friction adjustment mechanism to create sequential closing of the gripper for stronger more robust grasps. The cable routing is improved for more reliable opening by constricting the cable path through flexible joints on the PSSB.

- **Novel Cross-Shaped (Dual) and Reconfigurable Prestressed Spring Steel Band Gripper Designs:** We then create a reconfigurable gripper design that utilizes a cable routing and design similar to the first single PSSB gripper design. This design has a rotating base that allows for reconfiguration between a stacked configuration and cross configuration, allowing for more flexibility in grasping. We then create a cross-shaped gripper design based on the silicone encased single PSSB gripper design that has robust grasping and reliable opening.

- **Active Tuning of Gripper triggering Force with Nitinol SMA Springs:** We utilize Nitinol SMA springs to create on the fly triggering force adjustment of the silicone encased PSSB gripper, allowing for expanded flexibility in grasping. An open loop control method is used to control the SMA spring force, and the expected triggering force reduction is experimentally validated. The SMA springs make the gripper more robust for aerial grasping by controlling the triggering force of the gripper to reduce accidental gripper triggering during flight and more precise gripping of a variety of objects.

- **Versatile Grasping:** The passive bistable gripper designs, including the single-band and cross-shaped configurations, provide a robust aerial grasping solution without requiring a precise alignment. It operates within a broad offset range from the gripper's center. Furthermore, the grippers can successfully grasp cylinders of different diameters at various orientations. This range of successful grasping enables our grippers to be applied to various real-world scenarios.

Chapter 2

Single-Band PSSB Grippers

2.1 Introduction

It is important to understand why PSSBs are used for the gripper designs presented in this chapter. The material and mechanical properties of the gripper are integral to the functionality and performance of the gripper. The gripper must be made from a material that is both compliant and flexible while maintaining the ability to hold the weight of the drone. The bistability of PSSBs allows for passive grasping without needing energy to initiate or maintain a grasp, only requiring energy to open the PSSB. PSSBs have unique elastic, strength, and bistable properties that allow for passive, compliant, high-force grasping without the need for precise positional control. We first investigate single PSSB gripper design due to their relative simplicity with only one band.

In this Chapter, we will detail the design, testing, and experimental results of two separate single band PSSB gripper designs. We first detail the requirements and design parameters for the two single band PSSB grippers. We then discuss the design, experimental setup, testing, and experimental results for the first single band gripper, which we will call the first gripper. Then we will repeat this for the second, improved single band gripper, showcasing some of the differences and improvements between designs.

2.2 First Single PSSB Gripper

2.2.1 Design Requirements

Certain design parameters must be met for the gripper to be functional in a wide range of environments and applications. Ideally, the gripper will be able to quickly activate and secure the perch in around 0.15-0.3 seconds to reduce the chance of a failed perch [52]. Furthermore, the gripper must passively perch and be electronically resettable [18]. Some power is going to be required to initiate, but no power or electricity can be used to hold the perching position. If power

were needed to hold a perch, sustained perching could not be achieved. Additionally, less power could be used for other applications, like research, inspections, or surveillance, during the perch [16]. The gripper must require no control systems to activate the perching motion, simplifying the design and limiting the required components and overall mass of the system [19]. However, control systems will be needed for the detaching of the perch, flight control, and manipulation. Finally, the gripper must be compliant to accept differing perching environments including varying diameters, materials, and surfaces.

2.2.2 Design for First Single Band Gripper

Since the gripper is customized, we explain the design rationale in this sub-section. The gripper mainly contains three major components: a 210 mm $\times$ 27.5 mm $\times$ 0.5 mm pre-stressed spring steel band (PSSB) as fingers for grasping, a 3D-printed rigid base to hold the PSSB and other components, and a cable-driven system for opening the gripper (Fig. 2.1). The PSSB is initially straight but can curl to grasp an object (bottom of Fig. 2.1). The middle of the PSSB is connected to the base through a slider that slides linearly up and down to allow the PSSB to retract during grasping. The two sides of the PSSB are supported by two inner beams from the rigid base. If the PSSB is compressed by an impact force from an object between the two inner beams, the slider moves downward, causing the PSSB to curl rapidly once the force is greater than the triggering force F_{tr}. The PSSB can initiate the grasping process without additional actuators. Because the PSSB is flexible, it can adapt to the object's shape after it is curled to grasp.

Opening of the PSSB is realized through a cable-driven system actuated by a DC motor. Two fishing lines (illustrated as yellow and red in Fig. 2.1) with equal slack are spooled on a dual-cable spool attached to a $1000:1$ geared DC motor with a magnetic encoder (#2373, Pololu). The inner loop (red) will push the slider upward, while the outer loop (yellow) will flatten the PSSB. The cables can be unspooled and loosened for reuse. The inner cable loop is routed through a curved section to smoothly transit from the sliding mechanism to the spool. Both cable loops have approximately the same slack such that the flattening of the PSSB coincides with the extension of

the sliding mechanism. Both cables are routed to be inside a cable management box to ensure the cables will not be tangled during the release process.

The rigid base is designed for optimal cable routing, such that the PSSB is flattened with the smallest force possible by pulling the PSSB open with a vertical downward force (the yellow cables are routed downward through holes in the base as seen in Fig. 2.1). There are two outer beams at the two further ends of the base to facilitate the flattening of the PSSB because the PSSB should be bent past a straight shape to return and maintain the flattened shape. Therefore, we design the two outer beams to be 4 mm lower than the inner beams.

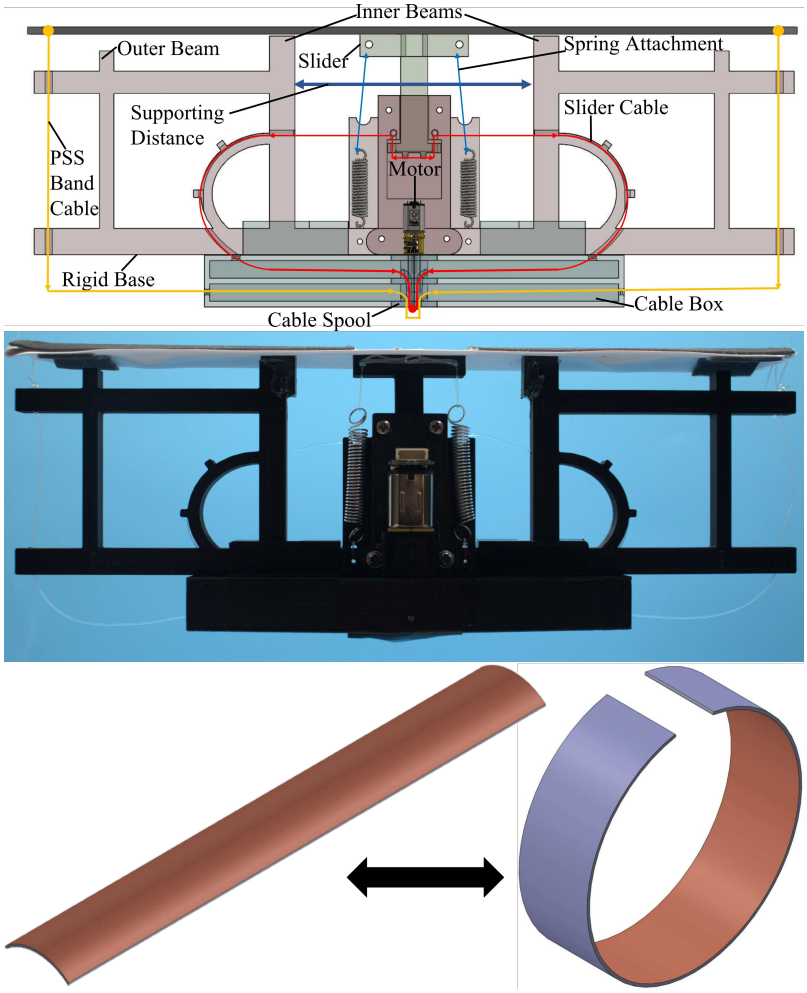

Figure 2.1: The design of the bistable gripper. Top: a detailed 3D model with major components labeled; middle: the prototype of the gripper; bottom: illustration of the two stable states of the PSSB placed on top of the gripper.

Two linear springs (50465A, $7/32$"x1", 14.55 mm, NEIKO) are used to apply pretension to PSSB to reduce the triggering force F_{tr}. The springs are attached from the base to the slider by fishing lines. The pretension can be manually adjusted by altering the displacement of the springs when the PSSB is flattened. The pretension in the springs can be estimated using $F_{Spring} = k\Delta x$, where $k = 0.274 \pm .009$ N/mm is experimentally obtained by measuring force and displacement three times using a force gauge (M5-2, Mark-10) and calipers.

2.2.3 Gripper Characterization

With the designed gripper, this section will detail the characterization of the gripper's triggering and opening force because these two forces will determine how we should control the manipulator arm so that the gripper can successfully grasp an object. For the triggering force, a small triggering force is desired for robust gripping and dynamic aerial grasping. Therefore, we will evaluate the influence of various parameters such as the distance between the two inner beams, spring

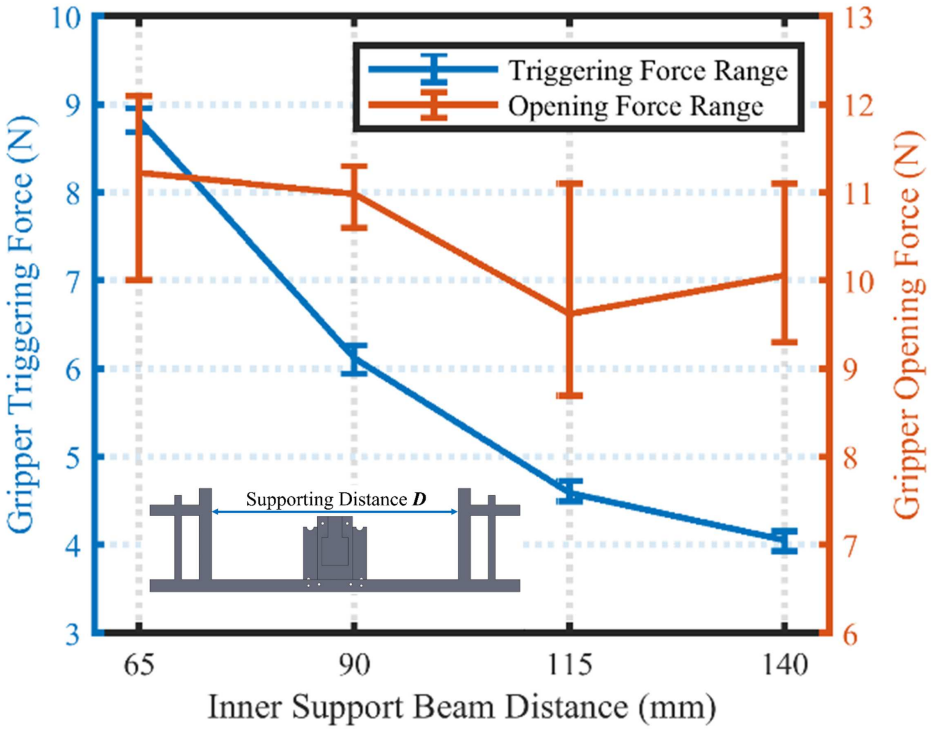

Figure 2.2: Triggering and opening force when the support distance between the two inner beams varies from 65 mm to 140 mm.

pretension force, and offset distance from the center. We also quantify the activation time since a fast activation is also desired because it will reduce the chances of a failed grasp of an object.

First, we examine how the support distance between the two inner beams will influence the triggering and opening force. The two inner beams support the PSSB as the sliding mechanism is pushed downward (Fig. 2.1), meaning the distance between them directly affects the triggering force. Four different rigid bases are 3D printed with inner beam distances of 65, 90, 115, and 140 mm. A force gauge (M5-2, Mark-10) is used to measure the triggering force with a test stand (ESM303, Mark-10). A 3D-printed base holds the gripper in the center of the test stand's lower jaw, and an 8 cm diameter cylinder is centered over the gripper in the top jaws. The gripper and cylinder are aligned so off-axis forces do not affect the results. The bottom of the cylinder is set 5 mm above the PSSB and lowered at a rate of 40 mm/min until the gripper is activated and the force levels off. The gripper is then reset, and the experiment is repeated five times for each support distance. The results of this experiment are plotted in Fig. 2.2, showing that the lowest triggering force is achieved at a 140 mm support distance. Figure 2.2 shows the triggering force can be approximated by a second-order polynomial in terms of support distance: $y = 0.008x^2 - 0.24x + 20.66$. This allows for the gripper design to be altered to achieve a desired triggering force before any pretension is applied.

To determine the effect of support distance on opening force, we test the opening force for the four rigid bases with no pretension force using another force gauge with a larger range (M2-20, Mark-10). The opening force is the force required to flatten both sides of the PSSB. Each rigid base is placed in a vice, with a fishing line running from either side of the PSSB through a pulley placed in the top jaws of the test stand to ensure equal force distribution to both sides of the band. The top jaw is raised at a speed of 330 mm/min until both sides of the PSSB are fully flattened, which is indicated by a distinct 'snap' sound. The experiment is repeated five times for each of the four bases. We record the maximum force during each experiment as the opening force and plot the results in Fig. 2.2, where the opening force decreases slightly between support distances of 65 and 115 mm before increasing slightly at 140 mm. Since the opening force does not vary greatly

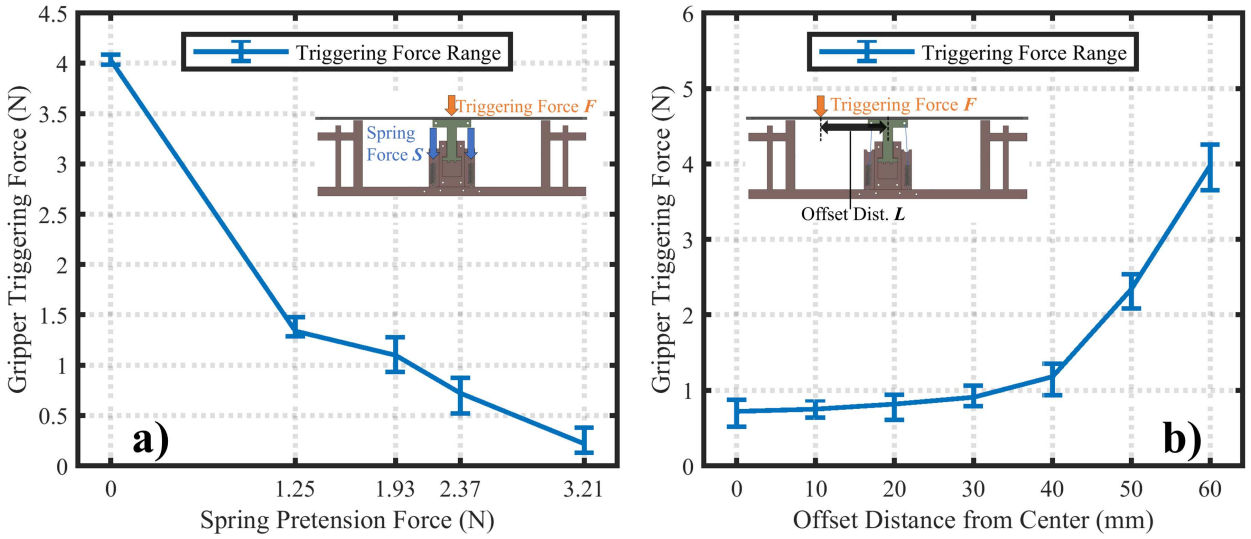

Figure 2.3: a) Triggering force with respect to four different spring pretensions (1.25 to 3.21 N) for 140 mm support distance. b) Triggering Force with respect to different offset distances (0 to 60 mm) from the center for 140 mm base with 2.37 N of pretension.

with the support distance, we do not need to consider this to choose a good support distance. Based on the results of triggering and opening forces, we choose the base with a support distance of 140 mm, as it provides the lowest triggering force before pretension is applied. Note that a slightly larger supporting distance might be possible, but it will not significantly decrease the triggering force.

The smallest triggering force we can obtain without pretension is 4.05 ± 0.11 N with a support distance of 140 mm. Since this value is still relatively large, we use linear springs to apply pretension to the PSSB. To determine the relationship between the pretension applied through the springs and the triggering force of the PSSB, five pretension forces values of 0, 1.25, 1.93, 2.37, and 3.21 N are applied. Note that these forces are not evenly distributed since we can only estimate the pretension force by manually changing the length of the string that connects the spring to the slider. We conduct experiments for the triggering force under the five different pretension forces. The results are shown in Fig. 2.3, exhibiting a steep drop in triggering force between no pretension and 1.25 N and a more gradual decrease between 1.25 and 3.21 N of pretension. From this experiment, we choose an ideal pretension range of 2 to 2.5 N, as this range allows for a triggering

force in the range of 0.5 to 1 N, which is small but stable (i.e., the gripper would not be triggered by external disturbance). Therefore, a pretension of 2.37 N is used for the remaining experiments.

For all the above characterizations, the triggering force is applied at the center of PSSB. The advantage of the developed gripper is that we do not need to precisely align the centers of the gripper and the object. In other words, the object can contact the PSSB at different locations, but successful grasping can still be ensured. This is important because the aerial grasping process is dynamic where the contact point is unlikely to be perfectly centered on the gripper. To assess the effect of contact locations on the triggering force, we test the triggering force again using the same methodology as above, with the contact location of a 8 cm cylinder being offset from the center of PSSB with an offset distance from 10 to 60 mm (step size: 10 mm). The results in Fig. 2.3 show that, at less than 40 mm, the offset distance has a small effect on the triggering force and, at larger than 40 mm, it has a large effect (the triggering force almost quadruples for a distance of 60 mm). This result suggests the gripper will still function and trigger as desired when the contact point is within an 80 mm range along the PSSB.

The grasping force of the gripper is also determined by fixing the gripper in the bottom jaws of the Mark-10, with cylinders of varying diameters (4, 6, 8, 10, and 12 cm) being placed in the top jaws. Using a force gauge with a large range (M2-20, Mark-10), the gripper is activated around the cylinder, then the cylinder is moved upwards by the Mark-10 until the gripper loses the grasp. This test was repeated 4 times for each cylinder, with the results being shown in Fig. 2.4, where the right shows the grasping force when the PSSB can overlap with itself, and the left shows the force when the PSSB is not able to overlap. The grasping force is much higher when the PSSB can overlap as it allows for direct friction between the bands, meaning that more force only increases the friction force between the bands. With smaller diameter cylinders, the gripper can hold upwards of 100 N of force, showcasing the high grasping force that the gripper can produce. The grasping force is larger with smaller diameter cylinders as the PSSB can more fully wrap around the object, and create overlap in some cases. Note that in Fig. 2.4, the grasping force for 6 CM diameter cylinder appears for both overlapping and non-overlapping results. This is because the PSSB will overlap

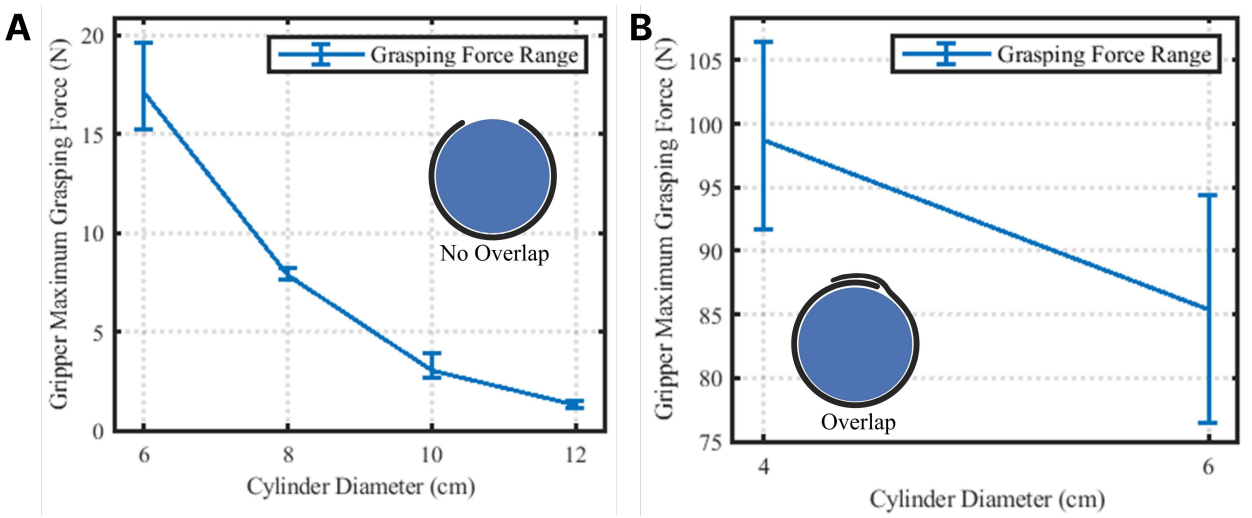

Figure 2.4: Maximum grasping force range for the first single band gripper design for 4, 6, 8, 10, 12 cm diameter cylinders, where: A) Grasping force for 6 to 12 CM cylinders when the PSSB does not overlap with itself, B) Grasping force for 4 and 6 CM cylinders where the PSSB does overlap with itself.

on the 6 cm cylinder sometimes, but doesn't consistently overlap, creating 2 different grasping force ranges that are both shown in Fig. 2.4. This inconsistent closing is investigated more closely in the next section where a sequential closing method is developed.

Finally, a quick gripper activation is desired for the best results when performing dynamic aerial grasping. We test the activation time using an 8 cm cylinder at four different locations: centered, 15 mm, 25 mm, and 35 mm offset from the center of the PSSB. The cylinder is placed on the PSSB and is pressed down until the gripper is triggered. The activation process is filmed using a high-speed camera at 240 frames per second (fps). The time $t = 0$ is set on the first frame when the PSSB can be seen moving and is stopped on the first frame when the PSSB has stopped curling. The results of this experiment provide an activation time accurate to $\pm.005$ seconds. Each test is repeated five times, and the average times during activation are represented in Fig. 2.5. The results in Fig. 2.5 suggest that the activation time increases with respect to the offset distance with the longest activation time being $0.17 \pm.005$ s. This is because one side of the PSSB needs more time to curl around the object when the offset distance is larger. However, the maximum activation time is still within the ability of the adaptive control system to position the drone in the correct proximity to the object being gripped during the entire activation process.

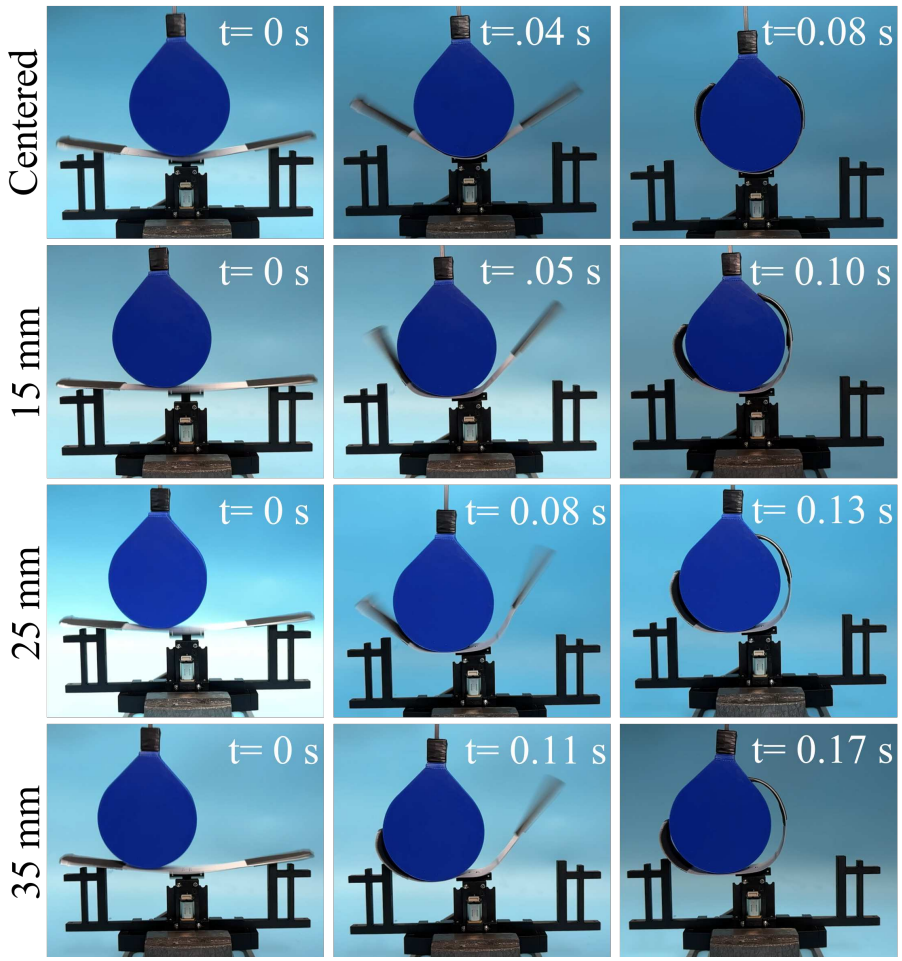

Figure 2.5: Activation time for gripper with an 8 cm cylinder with 0, 15, 25, and 35 mm offset from the center.

Additionally, the Adaptive Robotics Lab partnered with Dr. Spandan Roy's team from the Institute of Information and Technology (IIIT) Hyderabad to test this gripper design for use on a drone with an adaptive control scheme that their team was working on [8]. The gripper was mounted to their drone system in Hyderabad and some testing was done to show the integration and validation of their control scheme. Fig. 2.6 shows the gripper mounted on the drone and conducting aerial grasping and maneuvering

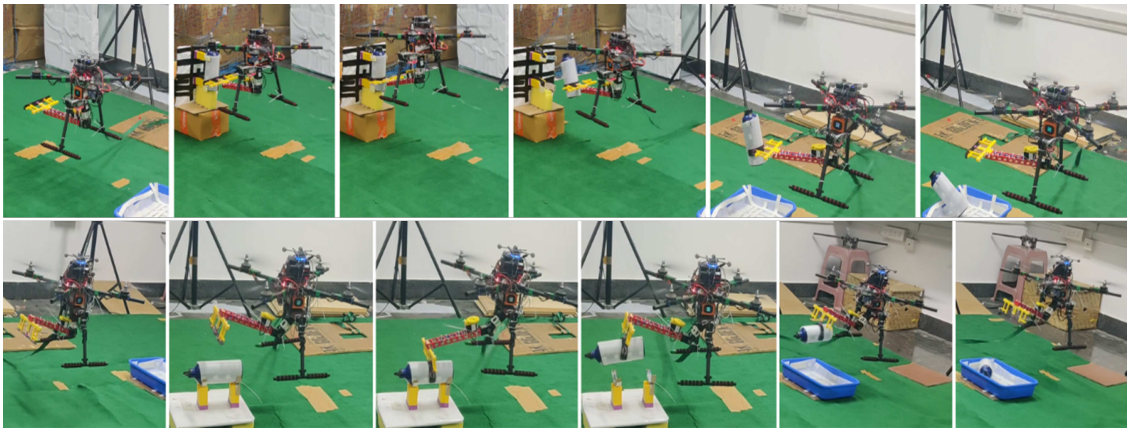

Figure 2.6: Top: Vertical aerial grasping with a drone, where the drone grasps a bottle, maneuvers, and then releases the bottle in the desired location. Bottom: Horizontal grasping where the drone grasps a bottle, maneuvers, then releases the bottle in the desired location. This figure was generated by Dr. Roy's Team from IIIT Hyderabad in partnership with the Adaptive Robotics Lab [8]

2.3 Silicone Encased Single PSSB Gripper

2.3.1 Design Requirements

The design and performance requirements for the silicone encased single PSSB gripper are the exact same as the first single PSSB gripper. The first single PSSB gripper design was a passive bistable gripper utilizing a PSSB for aerial grasping. The gripper was opened with a single motor and a cable network, making the gripper lightweight. This first single PSSB gripper design had two notable limitations. First, the gripper had reliability issues with consistent opening, as the cables from either side would snag and hinder proper opening. Second, the gripper did not close

sequentially, meaning that the two sides of the PSSB would often hit each other when closing, preventing the required overlap for a strong grasp. We address these limitations with the silicone encased single PSSB gripper presented in this section.

2.3.2 Design for Silicone Encased Single-band Gripper

For the silicone encased single PSSB gripper, one PSSB is attached to the base by a free-floating linear slider, allowing the PSSB to retract. The sliding mechanism and basic working principle for the gripper is identical to the first single PSSB gripper. The PSSB is supported on both sides by two vertical beams that extend out from the base. When an object contacts the PSSB between these beams with a sufficient triggering force, the slider moves downwards, and the PSSB curls rapidly to grasp the object. Grasping can be initiated without any actuator due to the PSSB's bistable nature, reducing complexity and weight.

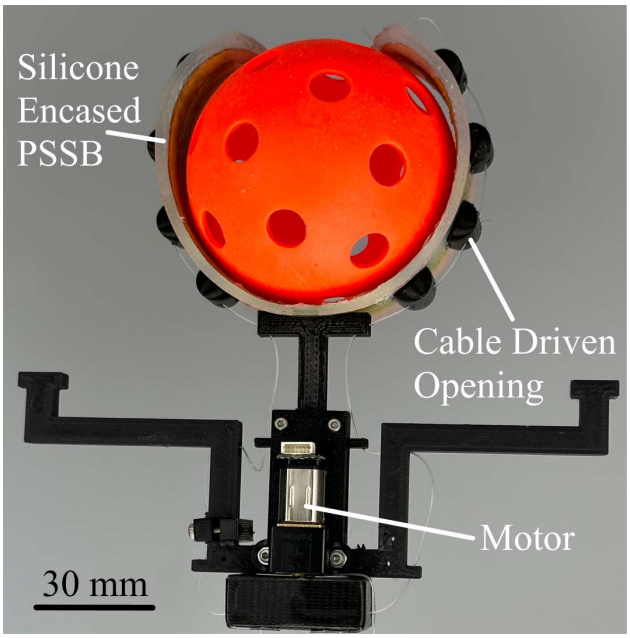

Figure 2.7: Brief overview of silicone encased single band PSSB gripper design

We enclose the PSSB with silicone (EcoFlex-30, Smooth-On) using a 3D-printed fully enclosed molding approach. The silicone can provide a flexible attachment for the flexible joints that can guide the cables to reliably open the gripper (Fig. 2.8) and provide shock absorption and protection

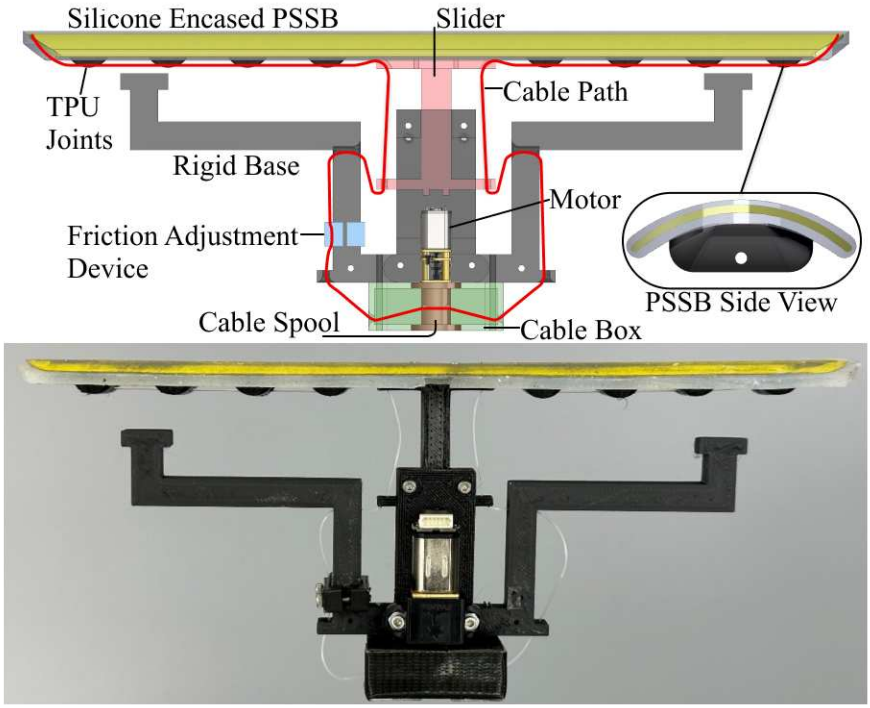

Figure 2.8: Design for the single-band gripper. Top: illustration of the main components including the cable path (red). Bottom: the prototype.

for the PSSB, gripper, and the object being grasped. The silicone enclosure is 2.5 mm thick on the bottom side of the PSSB, and 1 mm on the top side. Silicone is molded using a fully enclosed mold where the PSSB is screwed into the mold to fix it, with a curved void of 2.5 mm below and a 1 mm spacing between the top of the PSSB and the curved top of the mold. To open the PSSB, a cable-driven system is utilized to pull each side of the PSSB open (Fig. 2.7). The cables (fishing line) are routed through four 3D-printed flexible joints (thermoplastic polyurethane (TPU), 85A hardness) on the bottom of the gripper (Fig. 2.8). These joints are attached to the silicone on the bottom of the PSSB, approximately 12 mm apart, with a specialized silicone-TPU glue. A $1000:1$ geared DC motor with a magnetic encoder (#2373, Pololu) is used to wind the cable around a spool. The cable spool is enclosed in a box to ensure the cable does not get tangled during spooling and unspooling. The fishing line (illustrated by red in Fig. 2.8) is spooled to a set 'open' encoder position when the PSSB is fully flattened, then unspooled to its original position for rapid reuse. The line is routed from each end of the PSSB through the TPU joints, slider, and base, and to the cable box and spool.

This routing allows for simultaneously extending the slider while opening the gripper, increasing opening reliability, and reducing complexity compared to our previous gripper design where two cables are used.

To achieve better grasping results around smaller objects (6 cm diameter or less), the two sides of a PSSB should ideally curl at different speeds so that they can overlap around the object to provide a high friction holding force. Without a proper design, the PSSB may curl at the same speed for both sides and hit each other, preventing the desired overlap. To address this problem, we add a friction adjustment mechanism to one side of the base that slows down the curling of one side of the PSSB by increasing friction on the cable (Fig. 2.8), which facilitates sequential closing (Fig. 2.10). The mechanism functions by clamping the cable between a 3D printed piece and the base with friction tape (GM631, 3M) attached to each.

2.3.3 Gripper Characterization

With the designed gripper, this section details the characterization through four experiments. First, we characterize the triggering force at various offsets from the center of the gripper, where a lower force is desired for robust grasping without precise positional control and for potential future dynamic aerial grasping. Second, we quantify the activation time and sequential closing for the gripper. A quick activation time is preferred because it will decrease the instances of failed grasping, while sequential closing is desired to create an overlap of the PSSB around an object for a stronger grasp. Third, we test grasping performance on cylinders with various diameters and varying pitch and offset angles, which are important to quantify grasping performance in different scenarios. Finally, we demonstrate the gripper's grasping ability for various real-world objects. The experimental methods and results are detailed in each of the following subsections.

Triggering Force

We first determine the triggering force of the gripper at offset distances of 0, 10, 20, 30, 40, and 50 mm from the center of the PSSB. 50 mm is the max offset distance used because, after this, both grippers fail to activate as the offset location approaches the outside beam. An adjustable

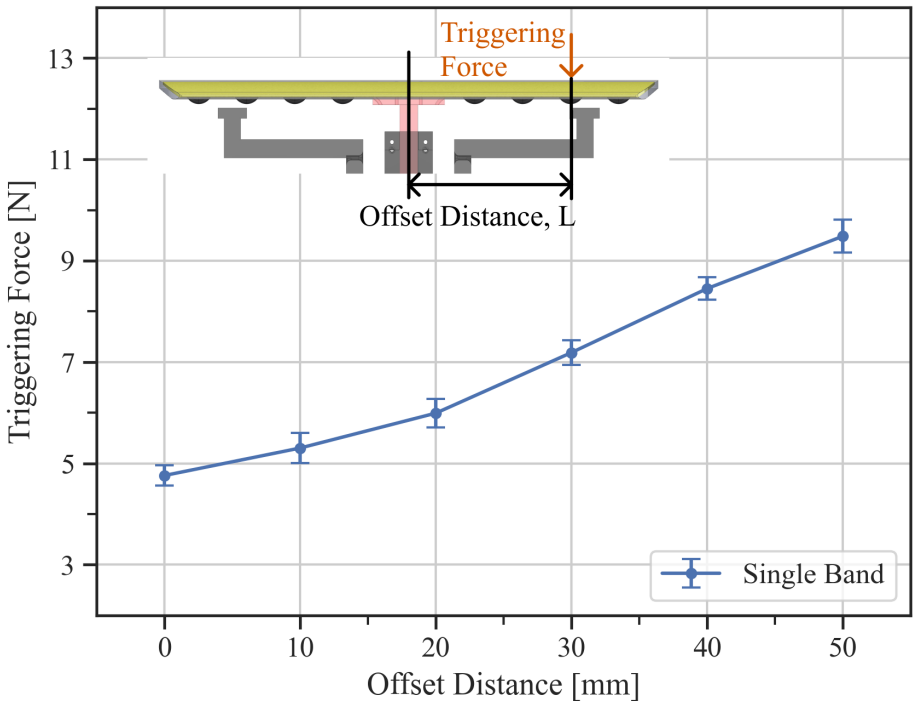

Figure 2.9: The triggering force with respect to offset distances varying from 0 to 50 mm with a step size of 10 mm with the average triggering force and variance between maximum and minimum shown for 5 tests

3D-printed base secures the gripper in the lower jaw of a test stand (ESM303, Mark-10) while triggering force is measured with a force gauge (M5-2, Mark-10) holding an 8 cm cylinder just above the gripper. The cylinder is lowered at 40 mm/min until the gripper is activated. The experiment is repeated five times for each offset distance. The results are plotted in Fig. 2.9, where the average triggering force for the single-band gripper starts at 4.67 N for 0 mm of offset and gradually increases to 9.48 N for 50 mm.

Activation and Sequential Closing

A quick gripper activation is desired to decrease the chances of a failed grasp due to the relative motion between the gripper and the object. We test the activation time using a thin rod with a 15 mm $\times$ 10 mm flat piece attached to its end to activate the PSSBs. The thin rod is used to avoid interference with the closing process of the PSSBs and make the closing process clearer on camera.

The flat end of the rod is placed on the center of the PSSB, aligned with the center of the slider, and pressed down to trigger the gripper. The activation sequence is captured using a high-speed

camera at 240 frames per second (fps). The activation time is the time from the PSSB first moving ($t = 0$) to stopping after fully curling and is accurate to $\pm.005$ s. Each test is repeated three times, with average times represented in Fig. 2.10. The single-band gripper closed on average in 0.14 s. The gripper's average activation times allow for quickly securing a grasp around an object as desired. The gripper can also open in 3 s for the single-band gripper enabling rapid reuse.

The recorded video is also used to show the sequential closing capabilities which allow for high-friction overlapping. For the single-band gripper, the right side of the PSSB will close first, in 0.10 s, followed by the left 0.04 s later at 0.14 s (Fig. 2.10). The left side of the PSSB will overlap the right every time the gripper is activated over five tests. The high-speed footage of the sequential closing can be seen in the supplemental video.

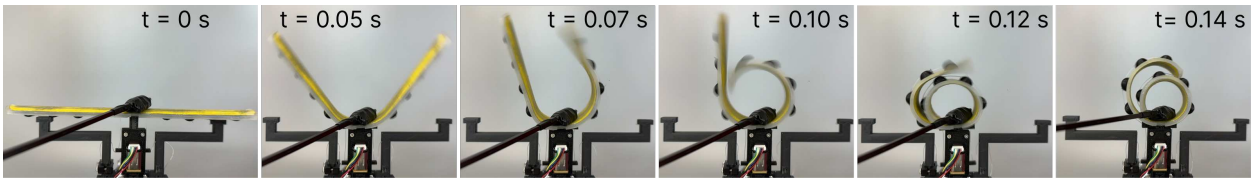

Figure 2.10: The sequential closing of the silicone encased gripper, where the left side will always close first, with the right then overlapping the left for a strong grasp.

Grasping Success Rate with Different Parameters

To determine the grasping abilities and parameters of the silicone encased single PSSB gripper, two experiments were conducted using cylinders with different diameters (4, 6, 8, 10, and 12 cm). The experiments are similar and aim to test the effect of different orientations of the cylinders on grasping success. First, we test the effect of offset angle (α) on grasping success. We then determine the effect of pitch angle (θ) on grasping success for the same cylinders.

The offset angle α is the horizontal angle from the axial centerline of the PSSB to the centerline of the cylinder upon impact (Fig. 2.11). The gripper is secured with the various offset angles labeled below it such that the center of the gripper is lined up over the origin of the angles. The cylinder is placed in the center of the band and rotated until the desired offset angle is reached. The

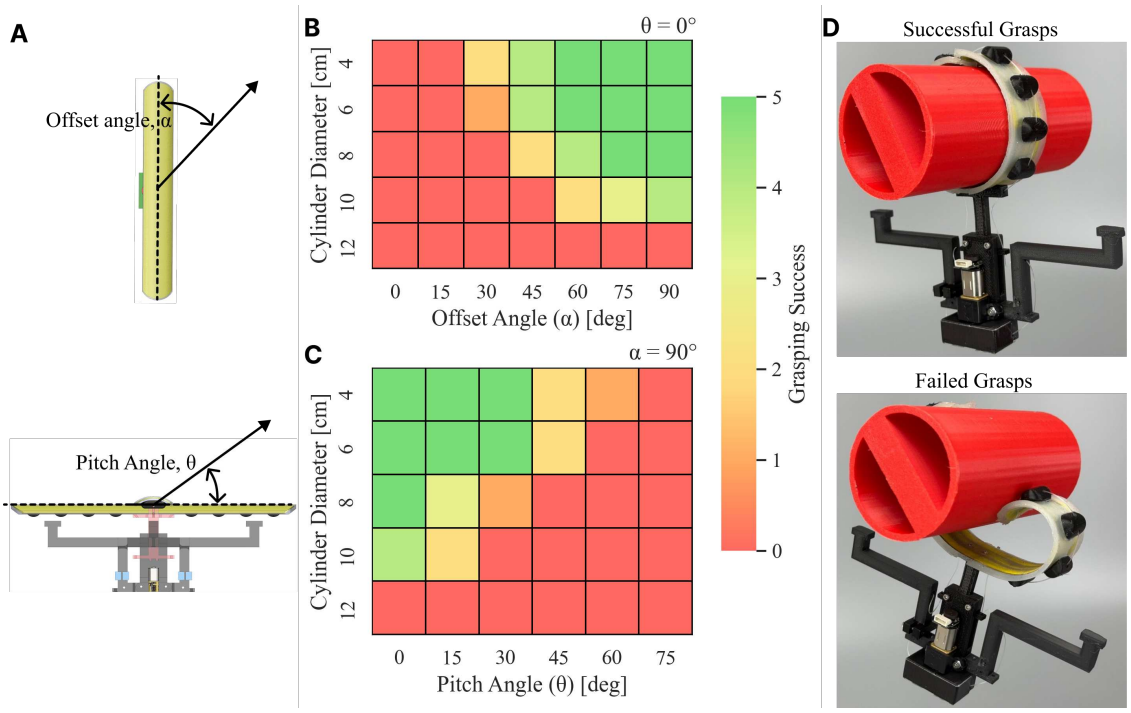

Figure 2.11: Experimental results for evaluating grasping success rate with different parameters. (A) Illustration of the offset angle α, and pitch angle θ; (B) Grasping success rate for the gripper out of five attempts for varying diameters vs. offset angle (for $\theta = 0$); (C) Grasping success rate for the gripper out of five attempts for varying diameters vs. pitch angle for $\alpha = 90$. (D) Representative images of successful and failed grasping conditions for the gripper.

cylinder is then pushed down using a guide until the gripper is activated. The gripper is then lifted upwards out of the vice and held. We consider the grasp successful if it can maintain the grasp around the object for 10 s without falling off. Representative images of successful and failed grasp can be seen in Fig. 2.11. Each test is repeated five times for each cylinder diameter and for each offset angle. For the single-band gripper, offset angles of $0 - 90$ with a step size of 15 are tested. Since the gripper is symmetrical in both directions, this range of offset angles covers all possible angles. The results can be seen in the first figure of Fig. 2.11. The single-band gripper has the highest range of grasping success rate for the widest range of cylinder diameters at $\alpha = 90$, with the success rate decreasing as α goes towards 15.

The pitch angle θ is the vertical angle from the axial centerline of the PSSB to the centerline of the cylinder upon impact (bottom of Fig. 2.11). The gripper is again secured and rested against a vertical board with the pitch angles labeled such that the center of the PSSB is lined up with the origin of the pitch angles on the board. The cylinder is placed on top of the PSSB and rotated upwards until it reaches the desired pitch angle, then pushed down using a guide until the gripper activates. The grasping success is defined similarly. This test is repeated for each cylinder diameter and pitch angle. We test a θ range of $0 - 75$. For the pitch angle test, we utilize the best offset angle for the gripper as determined from the previous experiment (90). The results can be seen in Fig. 2.11. The gripper performed well in this experiment, performing best at $\theta = 0$ (no pitch angle), with the grasping success rate decreasing as θ increased. The single-band had more successful grasping for angles less than 30.

Grasping real-world objects

We finally demonstrate the grasping ability of the silicone encased single PSSB gripper with many real-world objects, such as plastic water bottles, video game controllers, sunscreen bottles, screwdrivers, school glue, wiffle balls, and a 5-pound kettlebell. For these demonstrations, we first secure the gripper in an inverted position and then manually feed various objects to activate the gripper by hand. The objects are then left hanging in the gripper, with more than 30 s without falling being considered a successful grasp. The gripper is then tested for both vertical and hor-

Figure 2.12: Object grasping performance for the silicone encased single band gripper in the horizontal axis where: (Top) Horizontal grasping for the single-band gripper for (left to right) a video game controller, half-full plastic water bottle, full sunscreen bottle; (Middle) Horizontal grasping for (left to right) a wiffle ball, screwdriver, and 5-pound kettlebell; (Bottom) Vertical grasping for both grippers with (left to right) a game controller, a full plastic water bottle, and a full sunscreen bottle.

izontal grasping, where the PSSB is oriented facing sideways, and downwards respectively. The results can be seen in Fig. 2.12. The results show the ability of the gripper to grasp a wide variety of real-world objects with different weights and geometry. For horizontal grasping, the single-band gripper can grasp various objects successfully. It does, however, struggle with larger, heavier ob-

jects like the water bottle and video game controller (Fig. 2.12). The vertical grasping results for the gripper are shown in Fig. 2.12.

2.4 Conclusion

In this chapter, we presented two single PSSB gripper designs that can automatically initiate grasping upon contact with an object within a large offset distance. Both gripper designs can rapidly close and secure a grasp around objects. The first single PSSB gripper is tested for triggering force at varying offsets, effect of spring pretension on triggering force, grasping force, and activation time. The silicone encased single PSSB gripper has an improved design with a more compact and lightweight design. It also implements a friction adjustment mechanism to create sequential closing for more robust grasping. The cable routing is also improved for a more reliable opening. The silicone encased gripper is tested for triggering force at varying offsets, activation time, sequential closing, grasping success for varying parameters, and real world grasping scenarios.

Chapter 3

Cross-Band PSSB Gripper Configurations

3.1 Introduction

The silicone encased single band gripper design allowed for automatically initiating grasping upon contact with an object within a large offset distance with reliable opening and sequential closing. The gripper was able to grasp cylindrical objects well but struggled with spherical objects, heavier objects, and vertical grasping. To address these limitations, we explore a silicone encased cross-shaped gripper and a reconfigurable gripper design.

In this chapter, we will detail the design, testing, and experimental results of two separate PSSB gripper designs. We first discuss the design, experimental setup, and testing of a cross-shaped silicone encased PSSB gripper (Fig. 3.1). We then briefly detail the design and functionality of a reconfigurable gripper design that can transition from a 'stacked' position to a cross configuration on the fly. The requirements and design parameters for these grippers will be identical to those of the single band gripper designs.

3.2 Silicone Encased Cross-Shaped Gripper Design

The cross-shaped gripper integrates an additional perpendicular PSSB on top of the first (Fig. 3.2), with both bands connected to a free-floating dual-band slider for simultaneous activation. The rigid base is modified from the single-band base, with 2 additional vertical beams to activate the second PSSB. The additional beams sit 3 mm taller to accommodate different heights of the two PSSBs and also aid in sequential closing by triggering the upper PSSB, followed by the lower. To open the second PSSB, a second fishing line (illustrated by blue in 3.2), equal in length to the silicone encased single-band gripper, is used to flatten the band. The line runs from each end of the PSSB through the slider, base, and the dual cable box and spool, allowing for simultaneous spooling and unspooling of both cables without tangling. There are four TPU joints on each side

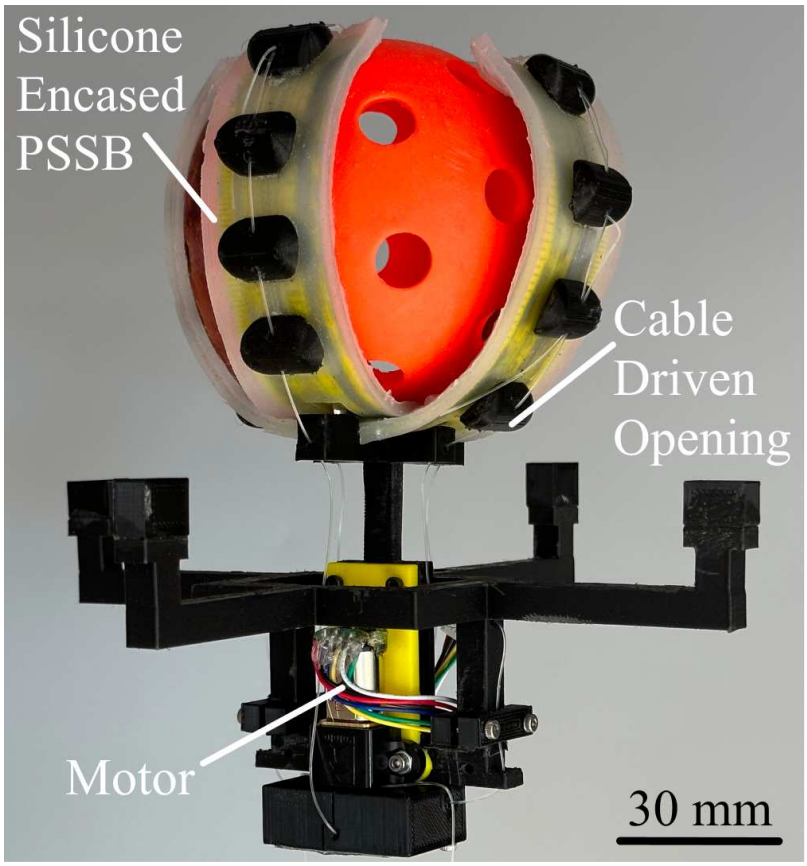

Figure 3.1: Design overview of the Cross-shaped gripper.

of the second PSSB that are identical in form and function to the single-band design. During the opening process, only the first fishing line will make the slider mechanism move upwards. Only the cable path of the second PSSB is shown in Fig. 3.2 in blue, as the first cable path is identical to the single-band gripper path (red in Fig. 2.8). Video of the opening process for the gripper can be seen in the supplemental video. To achieve sequential closing in the cross-shaped gripper, two friction adjustment mechanisms are added to the sides of the cross base with the cable path (red in Fig. 2.8) corresponding to the bottom PSSB in Fig 3.2. The friction mechanisms slow the closing of the first (bottom) PSSB. For good grasping, one PSSB would close with overlap, then the next would overlap on top of those. No friction adjustment mechanism is required for the second PSSB since its cable path (blue in Fig. 3.2) can enable the sequential closing for this band. This cable path behind the motor (left in Fig. 3.2) has two additional guide holes in the base compared to the

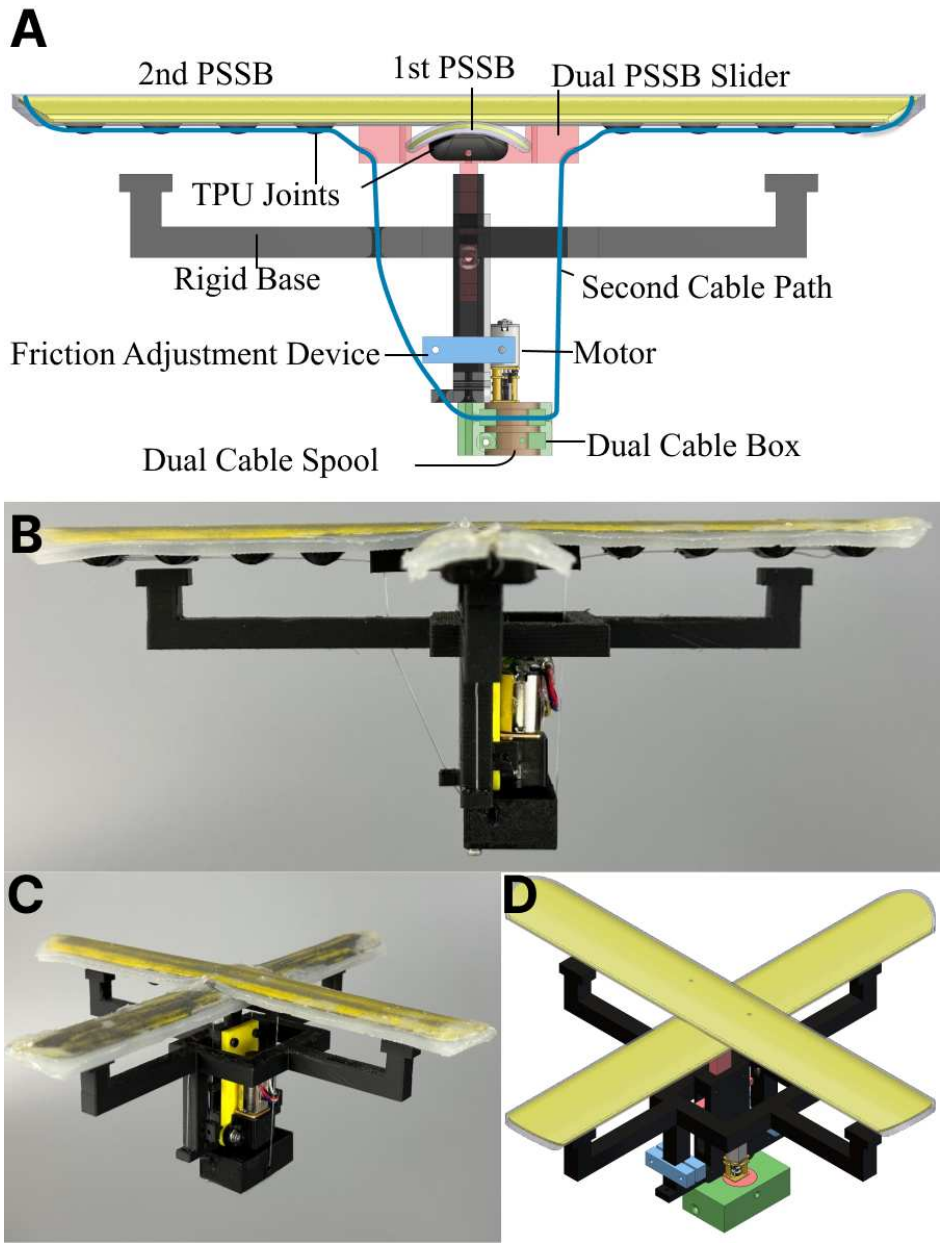

Figure 3.2: Design for the Cross-Shaped Gripper. (A) A solid model that details the design and components of the cross-shaped gripper including the cable path (blue) for the second PSSB; (B) and (C) Front and Isometric views of the cross-shaped gripper; (D) Isometric rendering of the cross-shaped gripper where component colors match the solid model in A.

front (right) side cable path, providing the required friction for the right side of the PSSB to close first (Fig. 3.4).

3.3 Characterization

With the designed gripper, this section details the characterization through four experiments. First, we characterize the triggering force at various offsets from the center of the gripper, where a lower force is desired for robust grasping without precise positional control and for potential future dynamic aerial grasping. Second, we quantify the activation time and sequential closing for the gripper. A quick activation time is preferred because it will decrease the instances of failed grasping, while sequential closing is desired to create an overlap of the PSSB around an object for a stronger grasp. Third, we test grasping performance on cylinders with various diameters and varying pitch and offset angles, which are important to quantify grasping performance in different scenarios. Finally, we demonstrate the gripper's grasping ability for various real-world objects. The experimental methods and results are detailed in each of the following subsections.

3.3.1 Triggering Force

We first determine the triggering force of the cross-shaped gripper at offset distances of 0, 10, 20, 30, 40, and 50 mm from the center of the PSSB. 50 mm is the max offset distance used because, after this, the gripper fails to activate as the offset location approaches the outside beam. An adjustable 3D-printed base secures the gripper in the lower jaw of a test stand (ESM303, Mark-10), while triggering force is measured with a force gauge (M5-2, Mark-10) holding an 8 cm cylinder just above the gripper. The cylinder is lowered at 40 mm/min until the gripper is activated. For the cross-shaped gripper, the offset distance used is along the bottom PSSB. The experiment is repeated five times for each offset distance. The results are plotted in Fig. 3.3, where the cross-shaped gripper gradually increases from an average triggering force of 6.22 N at 0 mm offset to 12.11 N at 50 mm offset.

The cross-shaped gripper has a triggering force only slightly larger than that of the single-band gripper. This might be due to the different stack heights of the two PSSBs and different beam heights that cause the sequential triggering. Although the measured triggering force is a bit large for grasping, we can potentially reduce this in our future work by applying pretension to the PSSB

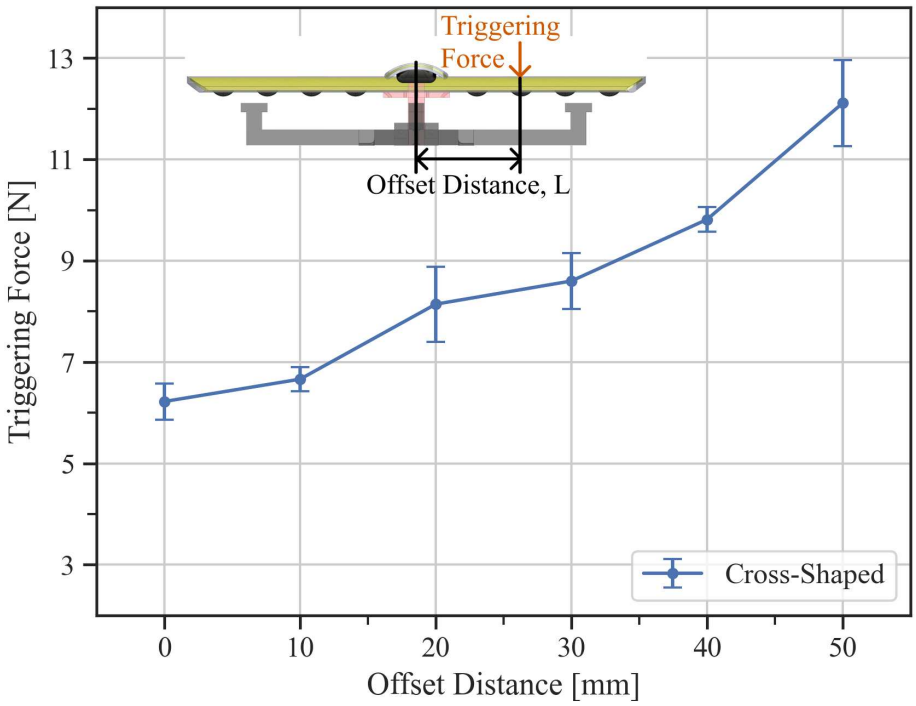

Figure 3.3: The triggering force with respect to offset distances varying from 0 to 50 mm with a step size of 10 mm for the cross-shaped gripper with the average triggering force and variance between maximum and minimum shown for 5 tests.

using springs, as done in our previous work [8] as well as with Nitinol SMA springs, which is discussed further in Chap. 4.

3.3.2 Activation and Sequential Closing

A quick gripper activation is desired to decrease the chances of a failed grasp due to the relative motion between the gripper and the object. We test the activation time using a thin rod with a 15 mm $\times$ 10 mm flat piece attached to its end to activate the PSSBs. The thin rod is used to avoid interference with the closing process of the PSSBs and make the closing process clearer on camera. For the gripper, the flat end of the rod is placed on the center of the PSSB, aligned with the center

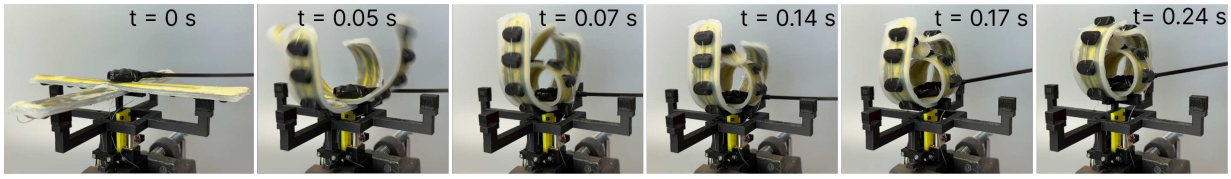

Figure 3.4: The sequential closing of the cross-shaped gripper.

of the slider, and pressed down to trigger the gripper. The activation sequence is captured using a high-speed camera at 240 frames per second (fps). The activation time is the time from the PSSB first moving ($t = 0$) to stopping after fully curling and is accurate to $\pm.005$ s. Each test is repeated three times, with average times represented in Fig. 3.4. The cross-shaped gripper closed in 0.24 s, slightly longer than the silicone encased single PSSB gripper, due to the delay for PSSB overlap. The gripper's average activation times allow for quickly securing a grasp around an object as desired. The grippers can also open in 4 s for the cross-shaped gripper, enabling rapid reuse.

The recorded video is also used to show the sequential closing capabilities of both grippers, which allow for high-friction overlapping. For the cross-shaped gripper, the second PSSB on top will close first, with the right side (front right in Fig. 3.4) in 0.07 s, and the left (back left in Fig. 3.4) overlapping it at 0.14 s. The first PSSB at the bottom will close after the second PSSB and overlap it, with the right (back right in Fig. 3.4B) at 0.17 s, and the left side (front left in Fig. 3.4) overlapping it at 0.24 s. The high-speed footage of the sequential closing can be seen in the supplemental video.

3.3.3 Grasping Success Rate with Different Parameters

To determine the grasping abilities and parameters of the cross-shaped grippers, two experiments were conducted using cylinders with different diameters (4, 6, 8, 10, and 12 cm). The experiments are similar and aim to test the effect of different orientations of the cylinders on grasping success. First, we test the effect of offset angle (α) on grasping success. We then determine the effect of pitch angle (θ) on grasping success for the same cylinders.

The offset angle α is the horizontal angle from the axial centerline of the PSSB to the centerline of the cylinder upon impact (Fig. 3.5). The gripper is secured with the various offset angles labeled below it such that the center of the gripper is lined up over the origin of the angles. The cylinder is placed in the center of the band and rotated until the desired offset angle is reached. The cylinder is then pushed down using a guide until the gripper is activated. The gripper is then lifted upwards out of the vice and held. We consider the grasp successful if it can maintain the grasp around the

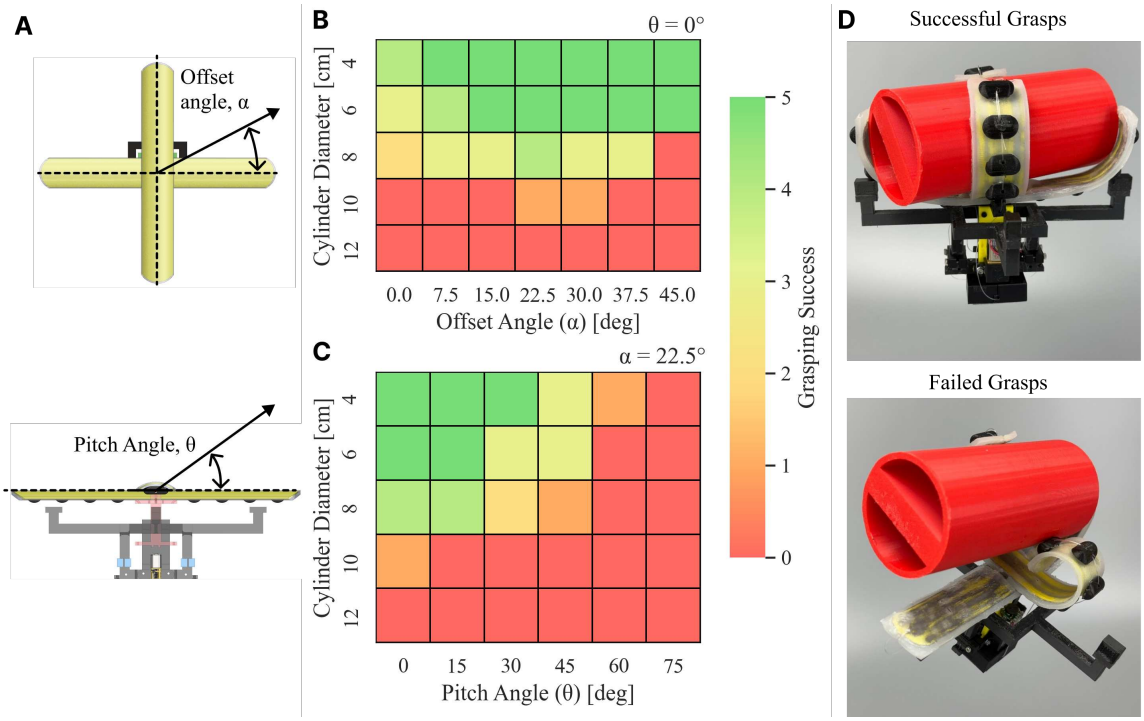

Figure 3.5: Experimental results for evaluating grasping success rate with different parameters. (A) Illustration of the offset angle α, and pitch angle θ; (B) Grasping success rate for the gripper out of five attempts for varying diameters vs. offset angle (for $\theta = 0$); (C) Grasping success rate for both grippers out of five attempts for varying diameters vs. pitch angle for ($\alpha = 22.5$). (D) Representative images of successful and failed grasping conditions for the gripper.

object for 10 s without falling off. Representative images of successful and failed grasp can be seen in Fig. 3.5. This test is repeated five times for each cylinder diameter for each offset angle. For the cross-shaped gripper, offset angles of $0 - 45$ with a step size of 7.5 are tested. Since the gripper is symmetrical in both directions, this range of offset angles covers all possible angles. The results can be seen in the first figure of Fig. 3.5. For the cross-shaped gripper, the success rate decreases as α goes towards 15. The cross-shaped gripper had the greatest grasping success rate for the widest range of diameters at $\alpha = 22.5$, with the success gradually decreasing as α goes towards 0 or 45. The grasping success rate is the highest at $\alpha = 22.5$ because one band can wrap around the cylinder, while the second acts as support. The cross-shaped gripper has a more consistent range of successful grasping than the single-band gripper, being able to securely grasp for any offset angle for diameters less than 6 cm, while the single-band gripper performs better with larger cylinders.

The pitch angle θ is the vertical angle from the axial centerline of the PSSB to the centerline of the cylinder upon impact (bottom of Fig. 3.5). The gripper is again secured and rested against a vertical board with the pitch angles labeled such that the center of the PSSB is lined up with the origin of the pitch angles on the board. The cylinder is placed on top of the PSSB and rotated upwards until it reaches the desired pitch angle, then pushed down using a guide until the gripper activates. The grasping success is defined similarly. This test is repeated for each cylinder diameter and pitch angle. We test a θ range of $0 - 75$. For the pitch angle test, we utilize the best offset angle for as determined from the previous experiment (22.5 for cross-shaped). The results can be seen in Fig. 3.5. The cross-shaped gripper performs best at $\theta = 0$ (no pitch angle), with the grasping success rate decreasing as θ increases. The cross-shaped gripper performed slightly better at angles above 30, while the single-band had more successful grasping for angles less than 30.

3.3.4 Grasping real-world objects

We finally demonstrate the grasping ability of the cross-shaped gripper with many real-world objects, such as plastic water bottles, video game controllers, sunscreen bottles, screwdrivers,

school glue, wiffle balls, and a 5-pound kettlebell. For these demonstrations, we first secure the gripper in an inverted position and then manually feed various objects to activate the gripper by hand. The objects are then left hanging in the grippers, with more than 30 s without falling being considered a successful grasp. The gripper is then tested for both vertical and horizontal grasping, where the PSSB is oriented facing sideways, and downwards respectively. The results can be seen

Figure 3.6: Object grasping performance for the silicone encased cross-shaped gripper in the horizontal axis where: (Top) Horizontal grasping for the gripper for (left to right) a video game controller, half-full plastic water bottle, full sunscreen bottle; (Middle) Horizontal grasping for (left to right) a wiffle ball, screwdriver, and 5-pound kettlebell; (Bottom) Vertical grasping for the gripper with (left to right) a game controller, a full plastic water bottle, and a full sunscreen bottle.

in Fig. 3.6. The results show the ability of both grippers to grasp a wide variety of real-world objects with different weights and geometry. For horizontal grasping, the cross-shaped gripper can successfully grasp the same objects as the single-band gripper, but it performs much better when holding larger, heavier objects like the game controller and water bottle (Fig. 3.6). The cross-shaped gripper also excels in vertical grasping, being able to hold a full water bottle, sunscreen bottle, and game controller, while the single-band gripper fails to grasp these objects. The vertical grasping results for the cross-shaped gripper are shown in Fig. 3.6.

3.4 Reconfigurable Cross-Band Gripper

The single band and cross-shaped gripper designs allow for grasping of a variety of objects in real-world applications. The single band grippers grasp cylindrical objects well while struggling with heavier objects, vertical grasping, and spherical objects. The cross-shaped gripper grasps spherical and vertically well but struggles with longer cylindrical objects. Each gripper works well for certain geometries and struggles with others. This presents issues for dynamic environments when multiple different objects might want to be grasped with the same gripper, as each of the gripper designs will have limitations on grasping. To allow for dynamic grasping of a larger variety of objects without needing to change the gripper, we explore a reconfigurable gripper design.

This section will describe the design and functionality of a reconfigurable gripper that can transition from a 'stacked' configuration to a cross-shaped one, allowing for on the fly flexibility and control of the gripper configuration for more robust grasping.

3.4.1 Reconfigurable Gripper Design

The reconfigurable gripper consists of a stationary base and a rotating base, with a PSSB connected to each through a rotational slider mechanism. The slider mechanism functions by having a stationary slider, attached to the stationary base, that is nestled within a rotating slider that is attached to the rotating base (Fig. 3.7). This design allows for the rotating PSSB to rotate freely and independently without disrupting the sliding mechanism for the stationary slider and PSSB. sta-

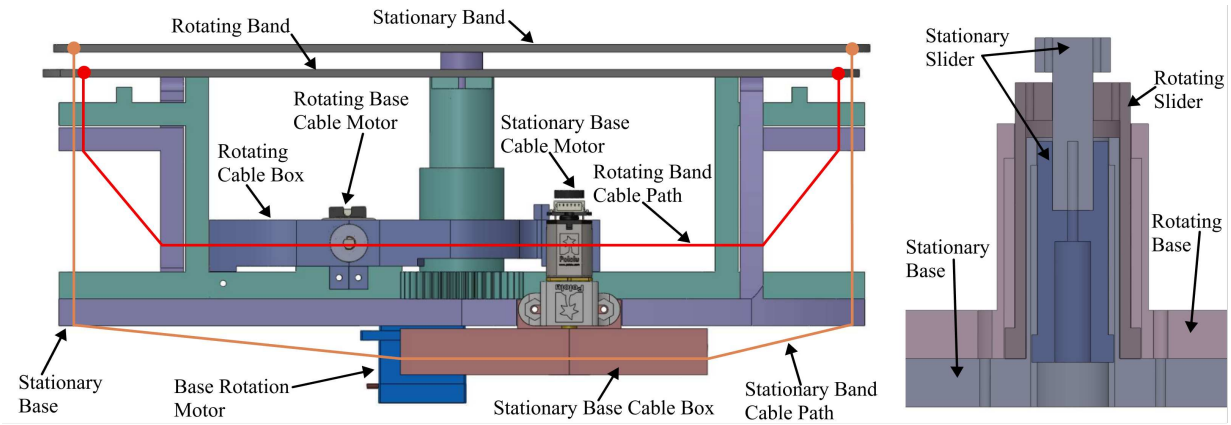

Figure 3.7: Design overview for the reconfigurable gripper including major components and cable paths

tionary PSSB is mounted to the stationary slider above the rotating slider and PSSB. The stationary base is purple in Fig. 3.7, while the rotating base is green. There are slots built into the stationary base for the rotating base to fit into such that both bases can be aligned and parallel. There is a continuous servo motor that is mounted to the stationary base that rotates the rotating base with a gear from 0 degrees up to 90 degrees, with the ability to stop at any point within that range. Each base has a separate cable box and motor for opening the gripper PSSBs, with the rotating cable box rotating with the base and the stationary cable box being fixed to the stationary base. The opening mechanism and process is identical to the first single PSSB gripper design, with the cables being routed through the outer parts of the base and through to the cable box. The cable routing for the rotating base is routed at an angle through the outer part of the base such that it doesn't snag or get caught on the stationary base. The cable path for each PSSB can be seen in Fig. 3.7 where red is for the rotating base, and orange is for the stationary base. The different grasping configurations and their applications are discussed further in the following section.

3.4.2 Grasping

The reconfigurable gripper has the ability to reconfigure itself to any orientation between the 'stacked' configuration (Left in Fig. 3.8) to a cross shape (Right in Fig. 3.8). This on demand reconfigurability allows for robust grasping of a variety of objects with different shapes and geometries. When in the 'stacked' configuration, the gripper can grasp cylindrical objects very well

(Left in Fig. 3.8), but struggles with longer objects and spherical objects. The X configuration grasps longer cylindrical objects, spheres, and varying geometries better than the stacked configuration, while also struggling with more spherical objects (Middle in Fig. 3.8). Lastly, the Cross configuration excels in grasping spherical or rounded objects but struggles with cylindrical and longer objects (Right in Fig. 3.8). Each configuration grasps certain geometries better than the other configurations, which allows for more robust grasping on the fly of multiple different objects by reconfiguring the gripper as needed. This allows for more applications, especially when considering grasping multiple different objects in a single flight where a traditional gripper would only be able to grasp certain geometries well. While the gripper does allow for more applications when grasping a variety of objects, there are reliability and tangling issues with the opening process that need to be addressed in the future.

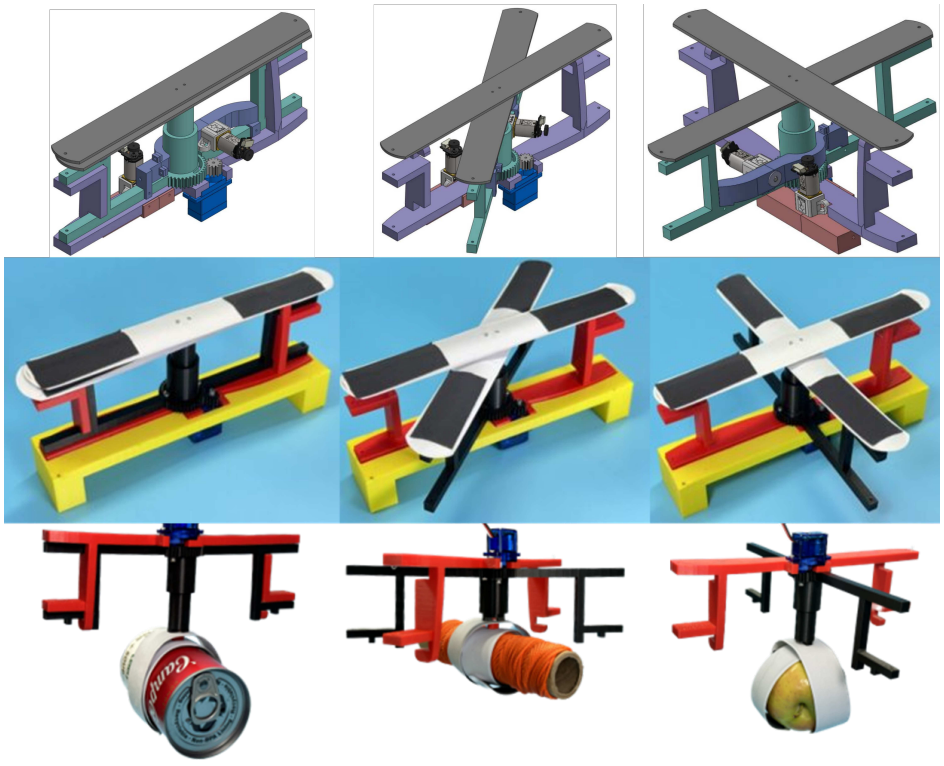

Figure 3.8: Three different configurations of the reconfigurable gripper including models and pictures of the gripper, and showcasing the grasping. From left to right: The gripper in a 'stacked' position, X position, and Cross position.

3.5 Conclusion

In this chapter, we presented two dual PSSB gripper designs that can automatically initiate grasping upon contact with an object within a large offset distance. Both gripper designs can rapidly close and secure a grasp around objects. The first silicone encased cross-shaped PSSB gripper is based on the single PSSB silicone encased gripper and is tested with the exact experiments and setup, with the cross-shaped gripper performing better at grasping spherical objects and with vertical grasping. It implements multiple friction adjustment mechanisms for controlled, sequential closing, creating robust grasping for a wide variety of grasping parameters. The reconfigurable gripper can adjust its configuration on the fly between a 'stacked', X, and cross configuration to adapt to grasping different geometries. Reliability issues with opening and tangling need to be addressed in the future for more reliable operation.

Chapter 4

Active Gripper Triggering Force Tuning

4.1 Introduction

Tuning the triggering force on the fly allows for greater control of the grasping process. When in flight, a high triggering force is advantageous to prevent accidental triggering of the gripper from acceleration. However the high triggering force also greatly increases the chances of failed grasps when grasping lightweight objects. The ability to tune the triggering force for grasping objects of varying weights and shapes allows for higher chances of a successful grasp. Tuning the triggering force also gives better flexibility for higher acceleration flight during aerial maneuvering.

In this chapter, we present the methods used to control the triggering force of the silicone actively encased single PSSB gripper using Nitinol SMA Springs (Nexmetal Nitinol 1-Way Memory Coil Spring W0.75 $\times$ D6.5 $\times$ C16; Af 45). The SMA springs are attached to the gripper in the same method as the first non silicone encased single PSSB gripper (Fig. 2.1) from Chapter 2. The springs will be connected on either side of the sliding mechanism to the rigid base. The SMA springs are wired in series to ensure consistent heating, as seen in Fig. 4.1.

We first attempt closed-loop control with a Proportional Integral Derivative (PID) system through controlling the resistance of the springs. This method had certain issues that will be discussed in further detail below, which led to using an open loop control method utilizing the timing of force generation. The rest of the chapter will first outline the closed loop control, open loop control, and then detail the real world applications of tuning the triggering force on the fly with SMA Springs.

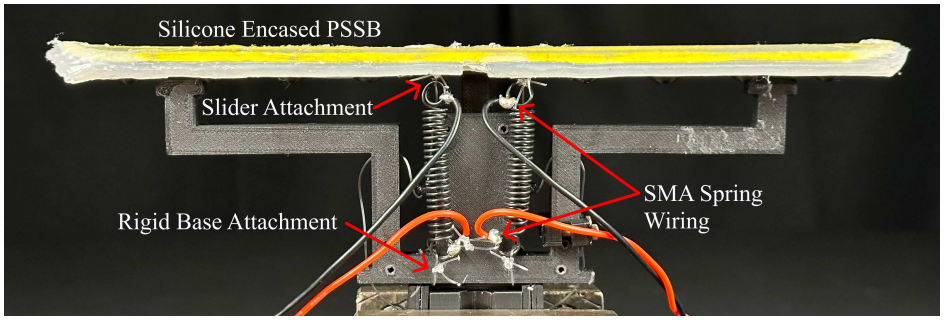

Figure 4.1: Configuration and attachment of the Nitinol SMA springs between the sliding mechanism and rigid base of the silicone encased single PSSB gripper.

4.2 Attempt on Closed Loop Control

4.2.1 Experimental Setup and Circuit Design

The closed-loop control utilizes a PID control method that relates the resistance through the springs to the estimated force generated by the SMA Springs. The resistance is calculated by determining the voltage and current going through the springs with an INA 219 Voltage and Current sensor connected to an Arduino UNO. The total resistance in the springs is very low (around 1.5 to $2.5\ \Omega$). Since the resistance is so low, any small voltage changes will greatly affect the calculated resistance. To maintain as constant of a voltage as possible, a DC-to-DC converter (LM2956) is used to regulate the voltage input from the power supply to the springs. Additionally, a MCP 2725 Digital to Analog Converter (DAC) is used to control the voltage output of the DC-DC converter with an Arduino UNO. The circuit design for the closed loop approach can be seen in Fig. 4.2, where the power supply is connected to the DC-DC converter, with a common ground to the Arduino UNO. The DC-DC converter output voltage can be controlled by the DAC input from the Arduino. This output voltage then goes through the current and voltage sensor, which is then used to calculate real-time resistance. The SMA Springs are connected to the voltage and current sensor and then to the common ground. The Voltage, Current, Time, and Resistance values are exported to excel in real time using the serial monitor of the Arduino. The Arduino UNO controls the voltage output of the DC-DC converter through a PID control scheme using the calculated resistance as an input, where the target resistance correlates to the desired force generation through the trendline

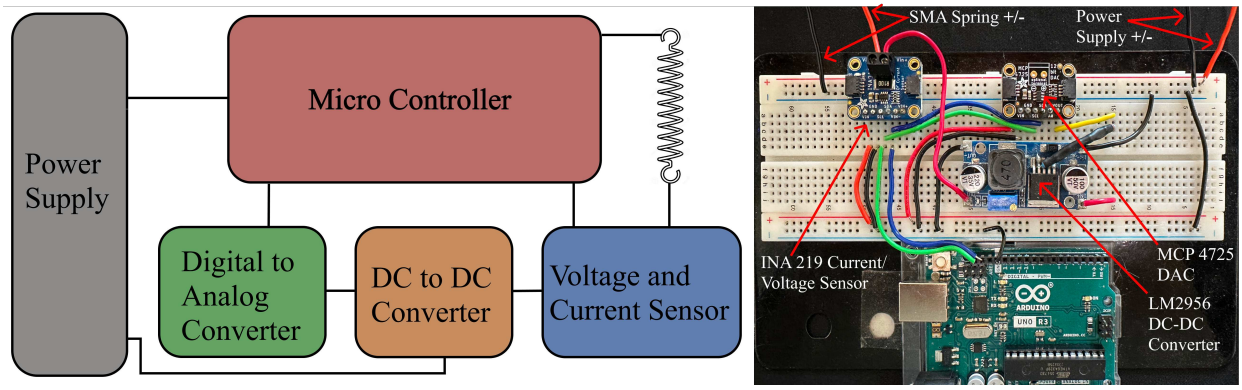

Figure 4.2: Circuit diagram for closed loop of Nitinol SMA spring force generation, including an INA 219 Current and Voltage sensor, MCP 4725 Digital to Analog Converter, LM2956 Dc to DC Converter, and Arduino UNO micro controller

seen in Fig. 4.3. Using this curve-fit, the force generated in the springs can be estimated from the resistance, allowing for the PID control to control the voltage output of the DC-DC converter to control the resistance, and thus the force.

To determine the relationship between resistance and force in the SMA springs, the SMA springs were connected to a constant 1.8 V while measuring the force and calculating the resistance with the measured voltage and current. The SMA springs are mounted between the upper and lower jaws of a Mark-10 force gauge (M5-2, ESM303 Test Stand). The springs are mounted such that their total displacement is 30 mm, which is chosen as this is the total displacement the springs will have when mounted on the gripper. The test was conducted 3 times for 200 seconds, allowing for the spring to reach a steady state where the force remained relatively constant.

4.2.2 Results

The relationship between force and resistance can be seen in Fig. 4.3, where three tests, the average, and the $5th$ order polynomial curve-fit are shown. The goal of this experiment was to determine the average relationship between SMA spring force and resistance over 3 tests. The resistance initially changes rapidly with respect to force (2.6 to 1.9 Ω) as voltage is applied and the spring heats up, correlating to a force range of 0 to 0.7 N. As the springs continue to heat up, the

resistance changes much more slowly (1.9 to 1.6 Ω) with respect to force, with the force rapidly increasing from 0.7 to 2.5 N while the resistance changes slowly in comparison.

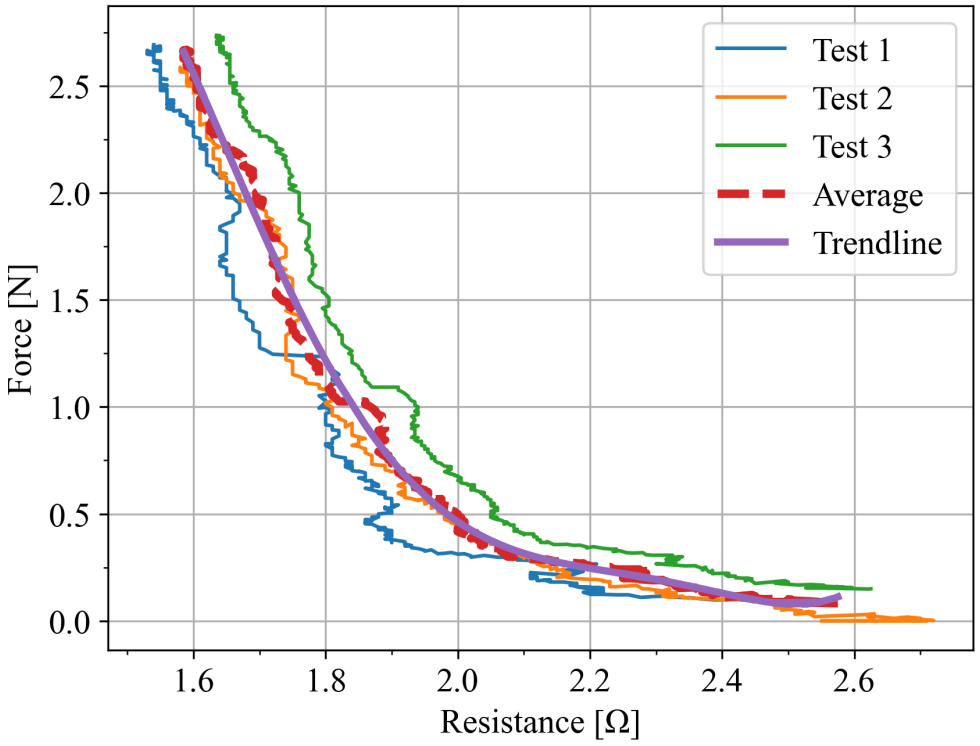

Figure 4.3: SMA Spring Force Vs Resistance while a constant 1.8 V is supplied, three tests and the average curve are shown, along with a $5th$ order polynomial curve fit of the data with the equation $F = 22.52x^5 - 235.35x^4 + 972.46x^3 - 1980.8x^2 + 1981.25x - 773.53$

The rapid change in force combined with the small change in resistance above 0.7 N presents challenges for the closed-loop PID control scheme. From 0.7 to 2.6 N, the resistance range is only around 0.35 Ω, meaning that a very small change of resistance (PID input) correlates to a large change of force (PID output). For example, 1.9 Ω correlates to about 0.7 N, while 1.8Ω correlates to around 1.4 N. A change of 0.1 Ω can cause a change in force of 0.7 N. This makes closed-loop control after 0.7 N of force very difficult. If we were able to precisely control the resistance within $0.01 - 0.02$ Ω, this small range of resistance change wouldn't cause any issues. This, however, is not possible for multiple reasons.

The accuracy and resolution of the INA 219 sensor is good, but still has some error, with a ± 0.06 V and ± 0.01 A accuracy for voltage and current, respectively. This is acceptable for most applications but is not ideal when the resistance is very small. The error values in voltage and current can create up to $\pm 0.07\Omega$ in resistance error. When a change of $0.1\ \Omega$ can cause a change in force of 0.7 N, this error makes this approach unfeasible. Additionally, the initial temperature of the SMA springs can affect the rate of change of the resistance, which can add to the error in the calculated values. For these reasons, we choose to explore the open-loop control method further.

4.3 Open Loop Control

The open loop control method utilizes the relationship between time and force generation in the SMA springs when a constant voltage is applied. This approach is used because it simplifies the control compared to the closed-loop approach. Additionally, the force generation is very consistent with respect to time. In this section, we first detail the experimental setup, testing, and characterization of the SMA springs for the open loop control scheme. We investigate the relationship between force and time, cool down and force, and SMA spring force and triggering force.

4.3.1 Force Time Relationship for Constant Applied Voltage

To control the SMA spring force generation with the open-loop control method, we must first determine the relationship between time and force generation when a constant voltage is applied. We first experimentally obtain a good constant voltage to apply to the springs for control. Ideally, for a good constant voltage, the steady state force will be large, while the rate of change of force with respect to time will be acceptable for controlling the force with timing. A high rate of change of force would create problems with controlling the force to a precise value, as the force will be rapidly increasing with time.

The same experimental setup is used as the closed-loop control approach, with the SMA springs, wired in series, mounted between the upper and lower jaws of the Mark-10 with 30 mm of total displacement. The voltage applied to the springs is set at a constant value, and the voltage is

applied for 150 seconds, allowing the SMA spring force to reach a steady state. The test is repeated 4 times for constant voltages of 1.4, 1.6, 1.8, and 2.0 V. The results can be seen in Fig. 4.4, where the average values are plotted and the shaded regions represent the range between maximum and minimum values for each voltage.

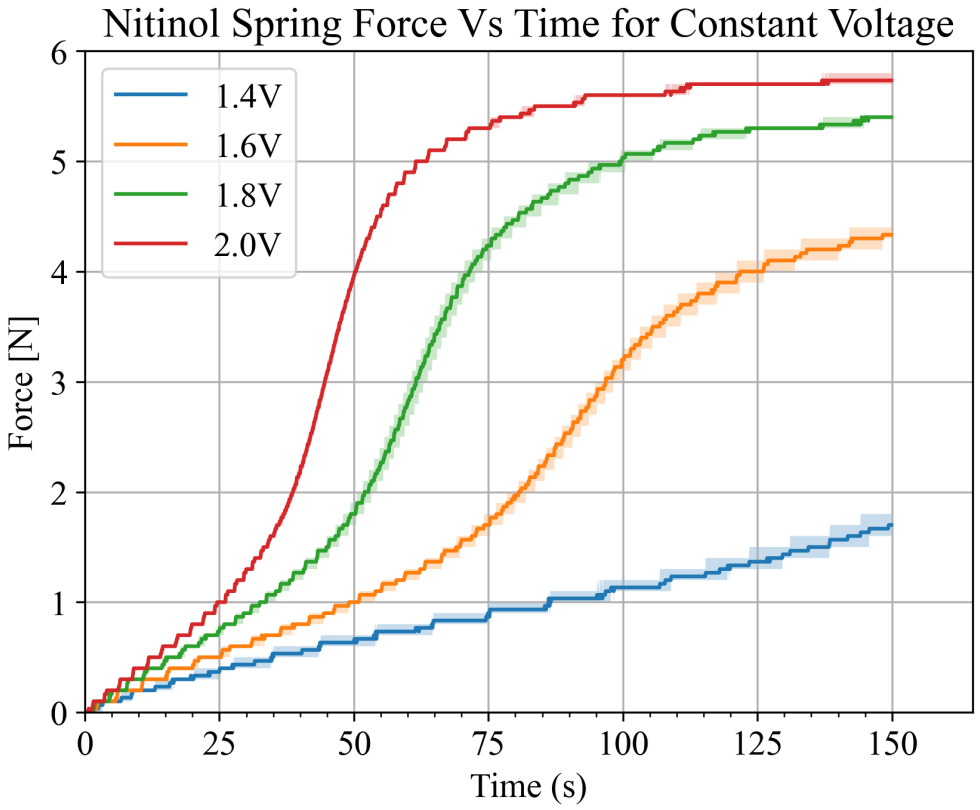

Figure 4.4: Range of Nitinol SMA spring force vs. time over 4 tests for 4 constant voltages of 1.4, 1.6, 1.8, and 2.0 V that are applied to the springs wired in series

The results show that force generation is very consistent with respect to time for constant voltages. The varying applied voltages do affect the steady-state SMA spring force, however. The steady-state force ranges from 1.8 N at 1.4 V to 5.7 N at 2.0 V. The steady-state force generation for 1.4 and 1.6 V is not as high as desired for meaningful triggering force reduction on the gripper, leaving 1.8 and 2.0 V. While 2.0 V produces a slightly higher total force in the springs than 1.8 V, the force increases at a very high rate between 2 and 4.5 N, making it hard to control the force with the relationship between force and time. For these reasons, we choose 1.8 V as the constant

voltage for our open loop control. With a constant 1.8 V applied, we can control the SMA spring force precisely by determining the time from the voltage being applied to when the SMA springs should reach the desired force. When the springs are attached to the gripper, this control will be utilized to apply voltage for a set amount of time before the gripper activates to reach the desired triggering force right as the gripper is triggering. To make the open-loop control feasible, the force cannot decrease rapidly when we stop applying the constant voltages. In this case, we need to look at the effect of cooling down after voltage is removed on force generation in the SMA springs.

4.3.2 Force Loss During Cool Down

Once the voltage is removed from the springs, they immediately begin to cool down. As the springs cool down, the force generated reduces. It is important to quantify this force reduction to understand its effect on the open loop control of the SMA spring force. If the force reduces rapidly after the voltage is removed, the time frame for grasping with the desired force is reduced. Ideally, the force will reduce at a similar rate once voltage is removed as it increases while voltage is applied. To characterize this, we use the same setup as the previous force-time relationship experiment. Since 1.8 V is the ideal constant voltage from Fig. 4.4, we apply this constant voltage for 4 varying times of 25, 50, 75, and 100 seconds before turning off the voltage source. The results can be seen in Fig. 4.5, where the average values are plotted and the shaded regions represent the range between maximum and minimum values for each voltage.

The results in Fig. 4.5 show that the effect of the cooldown on the SMA spring force is acceptable within the open loop control scheme. Once the voltage is removed, the force reduces at a similar rate to the increase in force while voltage is applied. At 25 seconds, the force reduces by 0.1 N after 5 seconds. The force is reduced slightly more after longer times of voltage being applied. The force reduces by 0.3 to 0.4 N after 5 seconds when voltage is removed at 50, 75, and 100 seconds. This means that if the object is grasped within around 5 seconds after the voltage is removed, the reduction in SMA spring force from the expected force will be very small at a maximum of 0.4 N difference.

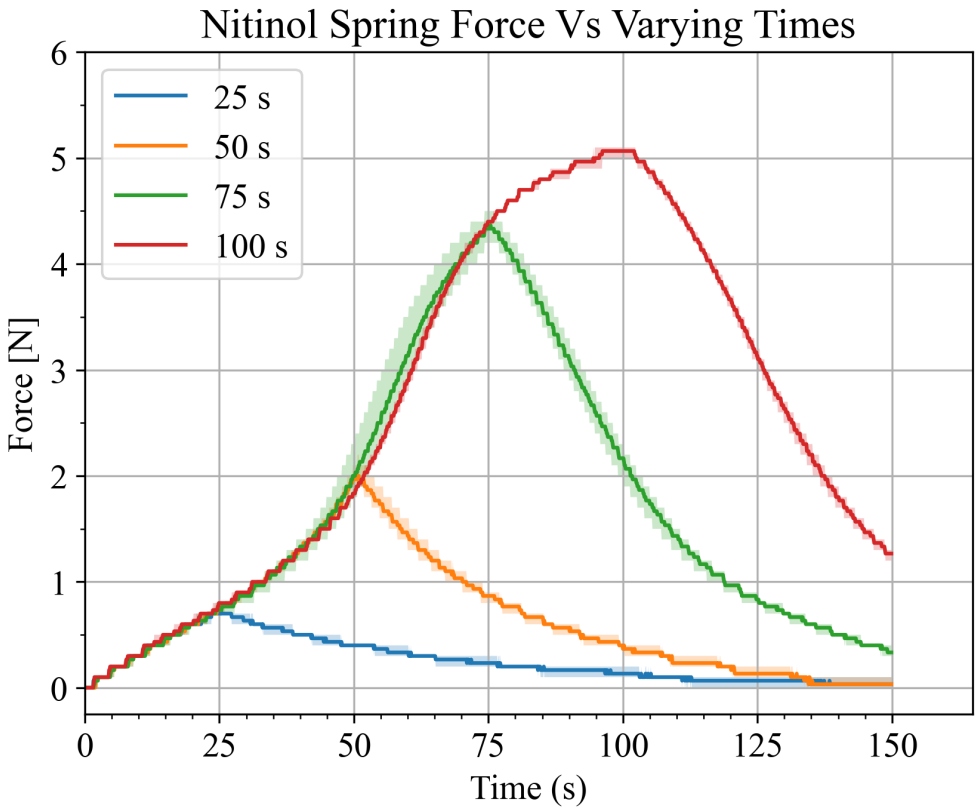

Figure 4.5: SMA Spring Force Vs Time for 1.8 V showing the effect of cool down once voltage is removed after 25, 50, 75, and 100 seconds on the SMA spring force generated.

Similarly, if the gripper is activated within 5 seconds before the desired time and force is reached the difference in force achieved and desired force is small. If the gripper were triggered 5 seconds early, at 20 seconds, the force difference would be about 0.1 N compared to at 25 seconds. At 5 seconds before 50, 75, and 100 seconds, the force difference for premature gripper activation would be around 0.3 to 0.4 N. For a ± 5 seconds range from the desired SMA spring force on activation, the maximum force variance will be 0.8 N. It will, however, likely be closer to 0.4 N as the ranges for 5 seconds before and after the desired activation are 0.4 N below the desired activation force. The variability in SMA spring force upon grasping is verified to be within an acceptable range from the results in Fig. 4.5, and we then verify the reduction of gripper triggering force with the SMA springs in the next section.

4.3.3 Reducing Triggering Force using Open Loop Control

In this section, we validate the open loop SMA spring force control method to control the triggering force in the silicone-encased single band gripper. The open loop method will be utilized to control the amount of force produced by the SMA springs to reduce the triggering force. We utilize the force-time relationship for constant 1.8 V from Fig. 4.4 to estimate the time needed at that voltage to reach the desired spring force. The expected gripper triggering force is the nominal triggering force with no offset from Fig. 2.9 of 4.67 N minus the expected SMA spring force. Using this relationship, the desired triggering force of the gripper can be tuned by controlling the timing of constant voltage being applied to the SMA springs. To validate this, we mount the silicone encased single band gripper in the bottom jaws of the Mark-10 (M5-2, ESM303 Test Stand), with an 8 cm cylinder mounted in the upper jaws such that it is aligned with the center of the PSSB and is placed 5 mm above it. The constant 1.8 V will then be applied for 0, 25, 50, 65, 75, and 100 seconds before the cylinder is lowered to measure the triggering force of the gripper. This is repeated 4 times for each of the 6 tests. The results can be seen in Fig. 4.6, where the triggering force range for each time lists the average, minimum, and maximum of 4 tests. The expected triggering force for each time is also listed.

The results show that the gripper triggering force correlates very closely to the expected triggering force. At 0 seconds, or when no voltage is applied, the SMA springs reduce the triggering force from 4.67 N to 3.5 N. For 0, 25, and 50 seconds, the expected triggering force is within the range of actual triggering forces. At 25 seconds, the average triggering force is 2.825, while the expected force is 2.80, with an average difference of 0.025 N. The average triggering force at 50 seconds is 1.65 N with the expected force being 0.15 N less at 1.5 N. The difference between the actual and expected triggering force is slightly larger at 65 and 75 seconds. The triggering force at 65 seconds is 0.675 N with the expected being 0.375 N less at 0.3 N. For 75 and 100 seconds, the expected triggering force is 0 N, although the actual triggering force is slightly higher at 0.35 N and 0.225 N respectively. The larger difference for 65, 75, and 100 seconds is most likely due to friction and heat loss between the SMA springs and the base that it is sliding along, although this

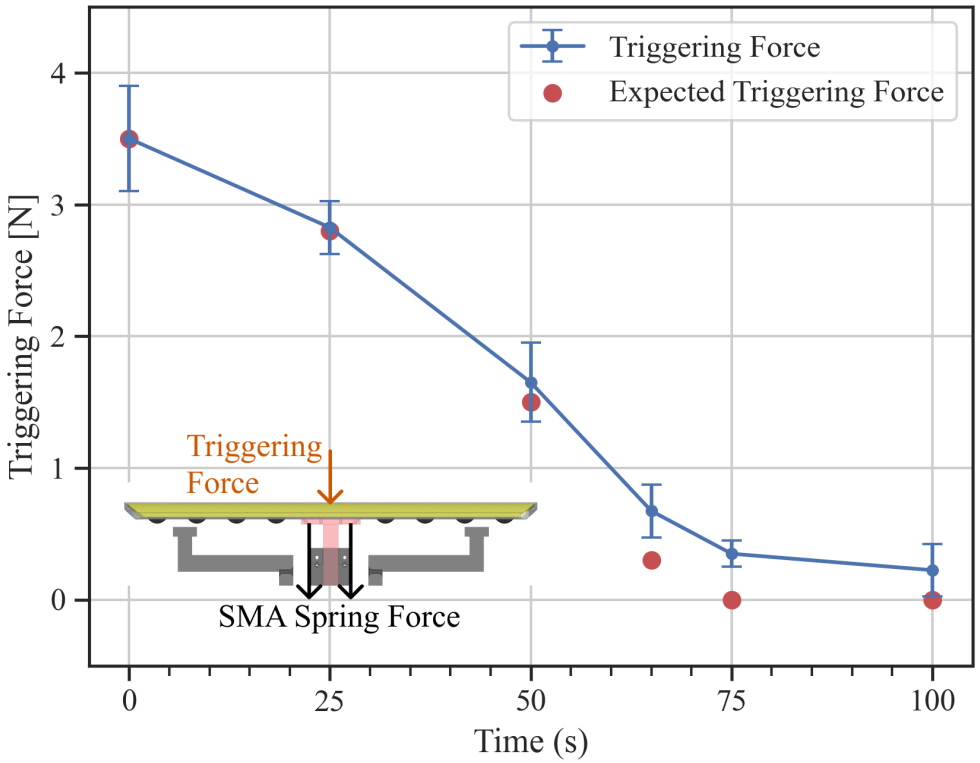

Figure 4.6: Triggering Force range for the gripper at 25, 50, 65, 75, and 100 seconds of constant 1.8 V being applied compared to the expected triggering force from Fig. 4.4

needs to be investigated further. Overall, however, the actual triggering force is very close to the expected triggering force, showing that we can very accurately predict and control the triggering force with this open loop control method. The open loop control method presented here can accurately be used to control the triggering force of the gripper for any desired triggering force range. Now, real world applications and benefits of on-the-fly triggering force tuning with SMA will be explored further.

4.4 Real World Application

It is important to verify our results from the open loop control with real-world applications of on the fly tuning of triggering force. On-the-fly tuning of the triggering force provides greater control over the grasping process. In flight, a high triggering force is advantageous to prevent accidental activation of the gripper due to acceleration. However, this high triggering force also

significantly increases the likelihood of failed grasps with lightweight objects. The ability to adjust the triggering force for objects of varying weights and shapes enhances the chances of a successful grasp. Additionally, tuning the triggering force offers better flexibility for high-acceleration flight during aerial maneuvers.

We will experimentally show this with 4 scenarios. First, we show that a high triggering force with no tuning will not be able to grasp a lightweight bottle. Then we show that by tuning the triggering force to be lower, the gripper can grasp the object. The importance of triggering force tuning during high acceleration flight is then shown. We first show that when the gripper triggering force is tuned to be higher the gripper can sustain rapid back-and-forth acceleration without premature triggering, and can successfully grasp a bottle. Then we show that when the triggering force is tuned to be lower, the gripper will activate prematurely and fail to grasp the bottle. The rest of this section will first outline the experimental setup, and then detail the results before concluding the chapter.

4.4.1 Experimental Setup

To experimentally show the real world applications, we first 3D print an adapter to mount the gripper to a 100 cm by 8 mm diameter metal rod. This adapter connects the base of the gripper to the metal rod for easy manipulation of the gripper. We then mount 2 supporting guides in a straight line for this rod that ensures pure linear, horizontal motion. These guides also ensure that the gripper PSSB is 50 cm from the plastic bottle before movement. This is important to ensure consistency between experimental trials. We then set a plastic bottle that is slightly filled (about $1/4$ to $1/3$ full) on an elevated stand such that it is level and centered with the center of the gripper. We then experimentally demonstrate the real world applications of tuning the triggering force through four scenarios. First, we test the gripper with high triggering force without tuning (0 seconds of 1.8 V applied). For this scenario, we move the gripper forward at a consistent speed from 50 cm away until the gripper makes contact with the bottle and either successfully grasps it or fails and pushes the bottle off the elevated stand. Next, for the same setup as before, we test

using the SMA springs to lower the triggering force (50 seconds of 1.8 V applied) to determine if the gripper can successfully grasp the bottle. This is repeated 3 times to verify the performance of the gripper for each scenario.

The applications and functionality of tuning the triggering force during high-acceleration flight are then determined. Using the same setup as before, we rapidly accelerate the gripper back and forth for about 2 seconds along the linear path to simulate these high acceleration movements before attempting to grasp the bottle. First, we test this when the triggering force is tuned to be slightly higher (50 seconds of 1.8 V applied), to test whether the gripper prematurely triggers before grasping. We then repeat this experiment for the gripper when the triggering force is tuned to be much lower (100 seconds of 1.8 V applied). The results of this experiment can be seen in Fig. 4.7.

4.4.2 Results

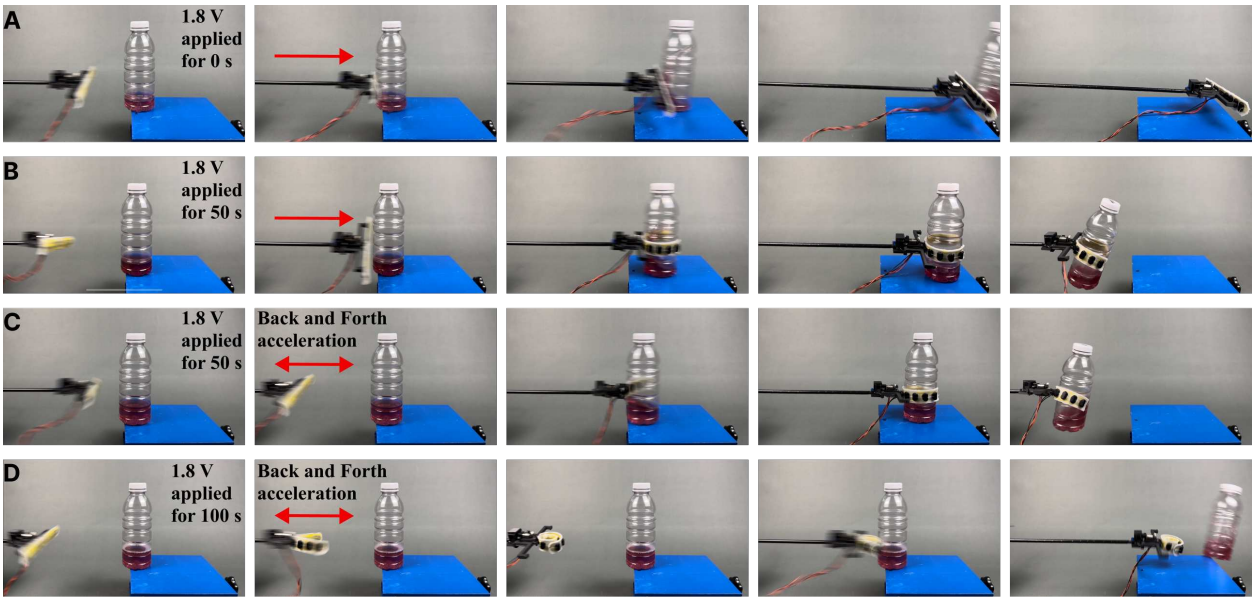

Figure 4.7: Real-world application of tuning the gripper triggering force with SMA springs, where: A) Failed grasping of a lightweight bottle when the triggering force is high and no voltage is applied, B) Successful grasping of a lightweight bottle when gripper triggering force is set lower by applying voltage for 50 seconds, C) Successful grasping of a lightweight bottle even after the gripper is accelerated rapidly back and forth where the gripper triggering force is set lower by applying voltage for 50 seconds, and D) Failed grasping of a lightweight bottle after the gripper is accelerated rapidly back and forth where the gripper triggering force is set to be very low by applying voltage for 100 seconds

The results in Fig. 4.7 show the importance and functionality of tuning the triggering force with SMA springs. Fig. 4.7A and 4.7B show the results of the real world application of using SMA springs to tune the triggering force for grasping objects. When the triggering force is not tuned, or 1.8 V is applied for 0 seconds, the gripper is unable to grasp the lightweight bottle as shown in Fig. 4.7A. The gripper is not able to grasp the object as the triggering force is too high and the bottle is pushed off the elevated stand. Conversely, when 1.8 V is applied for 50 seconds to tune the triggering force to be lower, the gripper can successfully grasp the bottle (Fig. 4.7B). This shows the application of tuning the triggering force, where the gripper is not able to grasp the bottle when no voltage or tuning is applied. When voltage is applied for 50 seconds, however, the gripper can successfully grasp the bottle.

Next, the application of tuning the triggering force during high acceleration flight on a drone is shown in Fig. 4.7C and 4.7D. First, when 1.8 V is applied for 50 seconds to tune the gripper to have a slightly lower triggering force, the gripper is rapidly moved back and forth and the gripper does not trigger prematurely and can grasp the bottle. Alternatively, when 1.8 V is applied for 100 seconds to significantly lower the triggering force, the gripper triggers prematurely when the rapid back-and-forth acceleration is applied and the gripper fails to grasp the bottle. This shows the importance of tuning the triggering force as high acceleration during flight will not prematurely trigger the gripper when the triggering force is tuned to be higher. When the triggering force is tuned to be lower, however, the gripper will prematurely trigger and the grasp on the bottle will fail. Overall, Fig. 4.7 shows the importance and application of tuning the triggering force of the silicone encased single PSSB gripper to ensure consistent grasping for varying environments, and to prevent premature triggering and failed grasping.‘

4.5 Conclusions

In this chapter, we first attempted a method of closed-loop control for force generation in nitinol SMA springs. To achieve this we utilized a PID control that had an input of calculated resistance from measured current and voltage to control the SMA spring force. There were multiple issues

with this approach, as above 0.7 N, the force changes rapidly compared to a very small change in resistance. Additionally, there were issues with the resolution and accuracy of the sensors we had available. This approach was deemed unfeasible and we then explored open loop control. The open loop method relies on the force-time relationship when a constant voltage is applied. We first determined the ideal constant voltage to apply of 1.8 V to produce high forces while maintaining control. Then we showed that the force reduction when voltage is removed is acceptable for a range of around 10 seconds. We then validate the open loop control method to accurately control and tune the triggering force of the gripper as desired, where the actual and expected triggering force correlates closely. The open loop control method is validated to provide precise tuning of triggering force on the fly, making it useful in a wide range of practical applications and expanding grasping possibilities.

We then explored the practical real world applications of on the fly triggering force. We demonstrate these real-world applications by showing that a high triggering force cannot grasp lightweight objects, whereas tuning and reducing the triggering force successfully achieves this. Additionally, we illustrate the benefit of a high triggering force in high-acceleration flight simulations, where the gripper does not trigger prematurely before grasping, unlike with a lower triggering force, which fails to grasp due to premature triggering. Adaptive, on-the-fly tuning of the gripper's triggering force provides significantly better control over the grasping process.

Chapter 5

Conclusions and Future Work

5.1 Conclusions

This thesis explored various gripper designs and control methods to enhance automatic grasping capabilities. Initially, two single PSSB gripper designs were developed to initiate grasping upon contact. The first design was tested for triggering force, spring pretension effects, grasping force, and activation time. An improved silicone-encased version featured a compact, lightweight design with friction adjustment for sequential closing, enhancing robustness. This version was tested for triggering force, activation time, sequential closing, and real-world grasping scenarios, showing significant improvements in reliability and performance.

We then explore cross-shaped PSSB gripper designs. We first design a cross-shaped gripper based on the single PSSB silicone-encased gripper. This gripper excelled in grasping spherical objects and vertical grasping, utilizing friction adjustment mechanisms for controlled, sequential closing. We then created a reconfigurable design that can reconfigure itself to any position between a 'stacked' position and a cross-shaped configuration. This gripper worked well, but has some issues with opening reliability and tangling. These designs demonstrated enhanced versatility and performance across various grasping parameters.

Adaptive on the fly tuning the triggering force of the silicone encased single PSSB gripper is then explored. We first attempted closed loop control using PID and resistance calculation. This was found impractical due to rapid force changes with small resistance variations and sensor accuracy limitations. Due to this, we then explore an open loop control method, which utilizes the force-time relationship under constant voltage. Testing identified 1.8 V as optimal for balancing force generation and control precision. The method showed consistent force generation and acceptable force reduction post-voltage removal. Validation experiments confirmed that the open loop method could accurately reduce and tune the gripper's triggering force, making it viable for

practical applications requiring on-the-fly adjustments. We show these real world applications by demonstrating that a high triggering force is unable to grasp lightweight objects, while tuning and reducing the triggering force is able to successfully grasp the object. We also show the benefit of a high triggering force by simulating high acceleration flight where the gripper will not trigger prematurely before grasping, while a lower triggering force will trigger prematurely and fail to grasp. Adaptive on the fly tuning of the gripper triggering force allows for much more control over the grasping process.

This thesis specifically contributes novel PSSB gripper designs to further expand research into aerial grasping and perching with drones. Furthermore, contributions were made investigating the possibility of using reconfigurable gripper designs and Nitinol SMA springs to adapt and tune a gripper on the fly to a variety of changing environments and applications. Overall, these advancements in gripper design and control methods contribute to more reliable and versatile automatic grasping systems, expanding their practical applications.

5.2 Future work

Future work on this research can be conducted in two aspects. First, we can improve the reconfigurable gripper design to make it more reliable and functional. It could then exhibit the advantages of both the single band gripper and cross-shape gripper to grasp a wide variety of objects or enable perching capability onto different objects. One approach for achieving this could be in the form of encasing the two PSSB's in silicone and adapting the opening mechanism and sequential closing abilities of the silicone encased gripper designs. This would create a much more reliable opening process and eliminate tangling of the opening cables. Additionally, the rotating base could be redesigned to be much smaller and more reliable in its rotation.

Second, we can place the gripper with active tuning capability onto a quadcopter to demonstrate the grasping capability under different conditions. We may even enable autonomous aggressive grasping by adding an onboard perception system (e.g., cameras) that can identify the object and

then plan the flying trajectory, tuning the triggering force before the grasping, and finally grasp the object, similar to what has been done using a soft gripper [53].

Bibliography

[1] E Kebadze, S.D Guest, and S Pellegrino. Bistable prestressed shell structures. *International Journal of Solids and Structures*, 41(11):2801–2820, 2004.

[2] Abdul Wadood. Brief overview on nitinol as biomaterial. *Advances in Materials Science and Engineering*, 2016(1):4173138, 2016.

[3] Haijie Zhang, Elisha Lerner, Bo Cheng, and Jianguo Zhao. Compliant bistable grippers enable passive perching for micro aerial vehicles. *IEEE/ASME Transactions on Mechatronics*, 26(5):2316–2326, 2020.

[4] Christian Geckeler and Stefano Mintchev. Bistable helical origami gripper for sensor placement on branches. *Advanced Intelligent Systems*, 4(10):2200087, 2022.

[5] Pham H Nguyen, Karishma Patnaik, Shatadal Mishra, Panagiotis Polygerinos, and Wenlong Zhang. A soft-bodied aerial robot for collision resilience and contact-reactive perching. *Soft Robotics*, 2022.

[6] Eric Deng and Yonas Tadesse. A soft 3d-printed robotic hand actuated by coiled sma. *Actuators*, 10(1):6, Dec 2020.

[7] Filippo Morra, Rezia Molfino, and Francesco Cepolina. Miniature gripping device. *Proc. IEEE Conf on Intelligent Manipulation and Grasping*, 01 2004.

[8] Rishabh Dev Yadav, Brycen Jones, Saksham Gupta, Amitabh Sharma, Jiefeng Sun, Jianguo Zhao, and Spandan Roy. An integrated approach to aerial grasping: Combining a bistable gripper with adaptive control. *arXiv preprint arXiv:2311.00769*, 2023.

[9] Jiawei Meng, Joao Buzzatto, Yuanchang Liu, and Minas Liarokapis. On aerial robots with grasping and perching capabilities: A comprehensive review. *Frontiers in Robotics and AI*, 8:739173, 2022.

[10] Marco Tognon, Hermes A Tello Chávez, Enrico Gasparin, Quentin Sablé, Davide Bicego, Anthony Mallet, Marc Lany, Gilles Santi, Bernard Revaz, Juan Cortés, et al. A truly-redundant aerial manipulator system with application to push-and-slide inspection in industrial plants. *IEEE Robotics and Automation Letters*, 4(2):1846–1851, 2019.

[11] Giuseppe Loianno, Vojtech Spurny, Justin Thomas, Tomas Baca, Dinesh Thakur, Daniel Hert, Robert Penicka, Tomas Krajnik, Alex Zhou, Adam Cho, et al. Localization, grasping, and transportation of magnetic objects by a team of mavs in challenging desert-like environments. *IEEE Robotics and Automation Letters*, 3(3):1576–1583, 2018.

[12] Alejandro Suarez, Victor M Vega, Manuel Fernandez, Guillermo Heredia, and Anibal Ollero. Benchmarks for aerial manipulation. *IEEE Robotics and Automation Letters*, 5(2):2650–2657, 2020.

[13] Boris Galkin, Jacek Kibilda, and Luiz A. DaSilva. Uavs as mobile infrastructure: Addressing battery lifetime. *IEEE Communications Magazine*, 57(6):132–137, 2019.

[14] HaoTse Hsiao, Jiefeng Sun, Haijie Zhang, and Jianguo Zhao. A mechanically intelligent and passive gripper for aerial perching and grasping. *IEEE/ASME Transactions on Mechatronics*, 27(6):5243–5253, 2022.

[15] Brycen Jones, Mahmud Hasan Saikot, and Jianguo Zhao. Bistable spring steel grippers for passive grasping. In *7th IEEE International Conference on Soft Robotics, RoboSoft 2024, San Diego, CA, USA, April 14-17, 2024*, pages 906–911. IEEE, 2024.

[16] Fabio Ruggiero, Vincenzo Lippiello, and Anibal Ollero. Aerial manipulation: A literature review. *IEEE Robotics and Automation Letters*, 3(3):1957–1964, 2018.

[17] Raphael Zufferey, Jesus Tormo-Barbero, Daniel Feliu-Talegón, Saeed Rafee Nekoo, José Ángel Acosta, and Anibal Ollero. How ornithopters can perch autonomously on a branch. *Nature Communications*, 13(1):7713, 2022.

[18] Rianna Jitosho, Kevin Choi, Adam Foris, and Anirban Mazumdar. Exploiting bistability for high force density reflexive gripping. In *2019 International Conference on Robotics and Automation (ICRA)*, pages 1241–1247. IEEE, 2019.

[19] Haijie Zhang, Jiefeng Sun, and Jianguo Zhao. Compliant bistable gripper for aerial perching and grasping. *2019 International Conference on Robotics and Automation (ICRA)*, 2019.

[20] Larry L. Howell. *Compliant mechanisms*. John Wiley Sons, 2002.

[21] Manish Kumar Mishra, Vikas Dubey, P. M. Mishra, and Isharat Khan. Mems technology: A review. *Journal of Engineering Research and Reports*, 2019.

[22] Qiaohang Guo, Huang Zheng, Wenzhe Chen, and Zi Chen. Modeling bistable behaviors in morphing structures through finite element simulations. *Bio-medical materials and engineering*, 23:S577–S582, 11 2013.

[23] J. A. von Fraunhofer, P. W. Bonds, and B. E. Johnson. Force generation by orthodontic coil springs. *The Angle Orthodontist*, 63(2):145–148, 06 1993.

[24] T Duerig, A Pelton, and D Stöckel. An overview of nitinol medical applications. *Materials Science and Engineering: A*, 273-275:149–160, 1999.

[25] D. Stoeckel. Nitinol medical devices and implants. *Minimally Invasive Therapy & Allied Technologies*, 9(2):81–88, 2000.

[26] Nuhu I. Abubakar, R.A. Application of niti shape memory alloy in ocean thermal energy conversion. *MRS Energy Sustainability (2024)*, 2024.

[27] Zonghao Zuo, Xia He, Haoxuan Wang, Zhuyin Shao, Jiaqi Liu, Qiyi Zhang, Fei Pan, and Li Wen. A nitinol-embedded wearable soft robotic gripper for deep-sea manipulation: A wearable device for deep-sea delicate operation. *IEEE Robotics Automation Magazine*, 31(1):96–107, 2024.

[28] Š. Ivošević. The prospects of application of shape memory materials in the marine environment. *International Conference on Smart Green Technology for Shipping and Maritime Industries*, 2021.

[29] D J Hartl and D C Lagoudas. Aerospace applications of shape memory alloys. *Proceedings of the Institution of Mechanical Engineers, Part G: Journal of Aerospace Engineering*, 221(4):535–552, 2007.

[30] Du Quan and Xu Hai. Shape memory alloy in various aviation field. *Procedia Engineering*, 99:1241–1246, 2015. 2014 Asia-Pacific International Symposium on Aerospace Technology, APISAT2014 September 24-26, 2014 Shanghai, China.

[31] T Ikeda. Ch. 11 - the use of shape memory alloys (smas) in aerospace engineering. In K. Yamauchi, I. Ohkata, K. Tsuchiya, and S. Miyazaki, editors, *Shape Memory and Superelastic Alloys*, Woodhead Publishing Series in Metals and Surface Engineering, pages 125–140. Woodhead Publishing, 2011.

[32] Zhao Guo, Yongping Pan, Liang Boon Wee, and Haoyong Yu. Design and control of a novel compliant differential shape memory alloy actuator. *Sensors and Actuators A: Physical*, 225:71–80, Apr 2015.

[33] Ji-Hyeong Lee, Yoon Seop Chung, and Hugo Rodrigue. Long shape memory alloy tendon-based soft robotic actuators and implementation as a soft gripper. *Scientific Reports*, 9(1), Aug 2019.

[34] J.M. Gallardo Fuentes, P. Gümpel, and J. Strittmatter. Phase change behavior of nitinol shape memory alloys. *Advanced Engineering Materials*, 4(7):437–452, 2002.

[35] J Eaton-Evans, J M Dulieu-Barton, E G Little, and I A Brown. Observations during mechanical testing of nitinol. *Proceedings of the Institution of Mechanical Engineers, Part C: Journal of Mechanical Engineering Science*, 222(2):97–105, 2008.

[36] Tony G Chen, Kenneth AW Hoffmann, Jun En Low, Keiko Nagami, David Lentink, and Mark R Cutkosky. Aerial grasping and the velocity sufficiency region. *IEEE Robotics and Automation Letters*, 7(4):10009–10016, 2022.

[37] William Stewart, Enrico Ajanic, Matthias Müller, and Dario Floreano. How to swoop and grasp like a bird with a passive claw for a high-speed grasping. *IEEE/ASME Transactions on Mechatronics*, 27(5):3527–3535, 2022.

[38] William RT Roderick, Mark R Cutkosky, and David Lentink. Bird-inspired dynamic grasping and perching in arboreal environments. *Science Robotics*, 6(61):eabj7562, 2021.

[39] Hai-Nguyen Nguyen, Robert Siddall, Brett Stephens, Alberto Navarro-Rubio, and Mirko Kovac. A passively adaptive microspine grapple for robust, controllable perching. *Soft Robotics Conference*, pages 80–87, 04 2019.

[40] Liam Kruse and Justin Bradley. A hybrid, actively compliant manipulator/gripper for aerial manipulation with a multicopter. In *2018 IEEE international symposium on safety, security, and rescue robotics (SSRR)*, pages 1–8. IEEE, 2018.

[41] Aurel X Appius, Erik Bauer, Marc Blöchlinger, Aashi Kalra, Robin Oberson, Arman Raayatsanati, Pascal Strauch, Sarath Suresh, Marco von Salis, and Robert K Katzschmann. Raptor: Rapid aerial pickup and transport of objects by robots. In *2022 IEEE/RSJ International Conference on Intelligent Robots and Systems (IROS)*, pages 349–355. IEEE, 2022.

[42] Joshua Fishman, Samuel Ubellacker, Nathan Hughes, and Luca Carlone. Dynamic grasping with a" soft" drone: From theory to practice. In *2021 IEEE/RSJ International Conference on Intelligent Robots and Systems (IROS)*, pages 4214–4221. IEEE, 2021.

[43] Xing Wang, Aarjav Khara, and Chao Chen. A soft pneumatic bistable reinforced actuator bioinspired by venus flytrap with enhanced grasping capability. *Bioinspiration & Biomimetics*, 15(5):056017, 2020.

[44] Sudhir Kumar Rajput, Abhishek Kaushal, Rabesh Kumar Singh, and Anuj Kumar Sharma. A study and fabrication of sma based 3d printed adaptive gripper. In *2021 Smart Technologies, Communication and Robotics (STCR)*, pages 1–5, 2021.

[45] Guddakesh Chandan, Brajesh Kanchan, R Premkumar, and R Karthik. Design and experimental analysis of gripper for shape memory alloy actuation. *International Journal of Engineering Research*, 5:2016, 04 2016.

[46] Nafise Faridi Rad, Aghil Yousefi-Koma, Hanie Rezaei, and Mohammad Ali Bazrafshani. Design and fabrication of a gripper actuated by shape memory alloy spring. In *2016 4th International Conference on Robotics and Mechatronics (ICROM)*, pages 455–458, 2016.

[47] R. Cortez-Vega, I. Chairez, A. Luviano-Juárez, and V. Feliu-Batlle. A hybrid dynamic model of shape memory alloy spring actuators. *Measurement*, 114:340–353, 2018.

[48] Sezer Var and Jovana Jovanova. Design of a soft underwater gripper with sma actuation. 11 2023.

[49] Andrija Milojević, Miša Tomić, Heikki Handroos, and Žarko Ćojbašić. Novel smart and compliant robotic gripper: Design, modelling, experiments and control. In *IEEE EUROCON 2019 -18th International Conference on Smart Technologies*, pages 1–6, 2019.

[50] Ferdinando Auricchio, Giulia Scalet, and Marco Fabrizio Urbano. A numerical/experimental study of nitinol actuator springs. *Journal of Materials Engineering and Performance*, 23:2420–2428, 2014.

[51] Deep Singh, Rutupurna Choudhury, Manidipto Mukherjee, and Yogesh Singh. Development of non-linear models to evaluate the niti sma spring actuator. *Journal of Mechanical Engineering and Sciences*, 16(1):8754–8769, Mar. 2022.

[52] R. Cortez-Vega, I. Chairez, A. Luviano-Juárez, and V. Feliu-Batlle. A hybrid dynamic model of shape memory alloy spring actuators. *Measurement*, 114:340–353, 2018.

[53] Samuel Ubellacker, Aaron Ray, James Bern, Jared Strader, and Luca Carlone. Aggressive aerial grasping using a soft drone with onboard perception, 2023.